UNIVERSITÀ DEGLI STUDI DI PADOVA

DIPARTIMENTO DI INGEGNERIA INDUSTRIALE

TESI DI LAUREA MAGISTRALE (LM) IN
INGEGNERIA DEI MATERIALI

SOLUTION PROCESSED P-I-N SOLAR CELLS BASED ON P3HT:PCBM BULK HETEROJUNCTIONS

Relatore: Prof. Massimo Guglielmi
Correlatori: Dott. Hendrik Bolink, Prof. Jorge Manuel Ferreira Morgado

Laureando: STEFANO VIRGILIO

ANNO ACCADEMICO 2011-2012

Acknowledgements

Several people contribute to the realization of this thesis, everyone in its own way, and I think that now it is time to highlight their merit.

Firstly a thanks to Dr. Hendrink Bolink, who proposed me this topic and kindly received me in his research group at Universitat de Valéncia, and to Alejandra, she patiently explained me how to prepare the devices and she always gave me good advices. Besides, the help and friendship of all the other people working at ICMol was also very important.

A special thanks to prof. Massimo Guglielmi, who accepted to be my adviser at Università di Padova and spent part of his valuable time following me. A thanks to prof. Jorge Morgado, to be my adviser in Instituto Superior Técnico of Lisbon.

To my parents and my family, for their efforts and their support in these years. They provided me the right conditions to purse my studies. Last but not least to all my friends, who brought me back the smile in the bad moments and with whom I shared good times.

Abstract

A high potential development in organic photovoltaic technology is the production of p-i-n structure, through the controlled doping of the active layer regions close to the electrodes. Here, an opening study on p-i-n structure formation by electrochemical doping with ionic liquids, namely 1-butyl-3-methylimidazolium hexafluorophosphate and tetra-n-butylammonium tetraphenylborate, on the P3HT:PCBM system was done. We demonstrate the possibility to increase the PCE of the device, even though a decrease of performance is also shown before the proposed formation of the p-i-n structure. The IL addition produces large changes in the morphology of the film before biasing. Upon formation of a p-i-n structure, a reduction of the non-geminate recombination and an increase of the charge carriers mobilities are observed. Active layer's thickness, ionic liquid concentration and nature of the ionic liquid are parameters that must be optimized in order to further increase PCE.

Key words

P3HT:PCBM, ionic liquid, 1-butyl-3-methylimidazolium hexafluorophosphate, tetra-n-butylammonium tetraphenylborate, electrochemical doping, p-i-n structure

Riepilogo

Uno sviluppo ad elevato potenziale della tecnologia fotovoltaica organica è la produzione di strutture p-i-n, realizzate grazie al dopaggio controllato delle zone dello strato attivo a contatto con gli elettrodi. In questa tesi si è realizzato un iniziale studio sulla formazione di strutture p-i-n tramite dopaggio elettrochimico con liquidi ionici, LI, specificatamente con 1-butil-3-metilimidazolo esafluorofosfato e tetra-n-butilammonio tetrafenilborato, in una miscela P3HT:PCBM. Si è quindi dimostrata la possibilità di aumentare l'efficienza di conversione energetica, ECE, di un dispositivo, nonostante l'iniziale diminuzione di efficienza riscontrata prima della formazione della struttura p-i-n. Si è inoltre osservato che l'aggiunta di LI produce importanti variazioni nella morfologia dello strato attivo. Dopo la formazione della struttura p-i-n, si è invece osservata una riduzione della ricombinazione non-geminata e un aumento della mobilità dei portatori di carica. Lo spessore dello strato attivo, la concentrazione e il tipo di LI aggiunto sono parametri che devono essere ottimizzati al fine di ottenere elevati valori di ECE.

Parole chiave

P3HT:PCBM, liquido ionico, 1-butil-3-metilimidazolo esafluorofosfato, tetra-n-butilammonio tetrafenilborato, dopaggio elettrochimico, struttura p-i-n

List of Figures

List of Tables

List of Abbreviations

A	Acceptor material	K	Kelvin
Å	Angstrom	λ	Wavelength
AFM	Atomic force microscope	LEC	Light emitting electrochemical cell
AM0	Air mass zero atmospheres	LUMO	Lowest unoccupied molecular orbital
AM1.5	Air mass at 1.5 atmosphere thickness	MEH-PPV	poly[2-methoxy-5-(2'-ethylhexyloxy)-p-phenylene vinylene]
bAm	tetra-n-butylammonium tetraphenylborate	MIM	Metal-insulator-metal
c	Speed of light	mIm	1-butyl-3-methylimidazolium hexafluorophosphate
CB	Conductive band	min	Minute
CB	Chlorobenzene	M_p	Maximum power point
$CF_3SO_3^-$	Triflate anion	n	n- doped region
C_g	Geometrical capacitance	η	Power conversion efficiency
cm	Centimeter	n_{phot}	Number of incident photons per unit time and unit area
CS	Charge-separated state	NREL	National Renewable Energy Laboratory
CT	Charge-transfer state	ns	Nanosecond
°C	Celsius degree	ODCB	Orto-dichlorobenzene
C_{60}	Buckminsterfullerene	OFET	Organic field effect transistor
C_μ	Chemical capacitance	OLED	Organic light emitting diode
D	Diode	OPV	Organic photovoltaic
D	Donor material	p	p- doped region
EA	Electron affinity	ns	Nanosecond
ECD	Equivalent circuit diagram	ODCB	Orto-dichlorobenzene
ECN	Energy research center for the Netherlands	OFET	Organic field effect transistor
E_{final}	Final energy	OLED	Organic light emitting diode
E_g	Energy gap	OPV	Organic photovoltaic
EQE	External quantum efficiency	p	p- doped region
eV	Electronvolt	π	Pi bond
FF	Fill factor	π*	Pi antibond
h	Planck's constant	P_{abs}	Absorbed power
HOMO	Highest occupied molecular orbital	PCBM	Phenyl-C61-butyric acid methyl ester
i	Intrinsic layer	PCDTBT	poly[N-9'-heptadecanyl-2,7-carbazole-alt-5,5-(4',7'-di-2-thienyl-2',1',3'-benzothiadiazole)]
I	Current	PEDOT	Poly(3,4-ethylenedioxythiophene)
IV	Current vs. voltage curve	PEO	polyethylene oxide
I_L	Ideal current source	P_{max}	Maximum produced power
I_{mp}	Current at maximum power point	PPV	Poly(p-phenylene vinylene)
I_{sc}	Short circuit current	PSS	poly(styrenesulfonate)
ITO	Indium tin oxide	P3HT	Poly(3-hexylthiophene)
J	Total current density	rms	Root mean square
J_{ph}	Photogenerated current density	R_L	Load resistor
J_0	Leakage current	RR	Regioregular
k	Boltzmann's constant	R_s	Series resistor

R_{sh}	Shunt resistor	V_{bi}	Built-in voltage
S	Siemens	V_{oc}	Open circuit voltage
σ	Sigma bond	V_{mp}	Maximum power voltage
TCO	Transparent conductive oxide	W	Power
T_g	Glass transition temperature	WF	Work function
V	Voltage	Ω/Sq	Sheet resistance
VB	Valence band		

Index

Chapter 1 -
Outlook on Organic Solar Cells

Introduction

In the last decade, photovoltaic energy production has grown at an incredible rate per year. Nevertheless, its contribution is still a small part of the overall energy need. Crystalline and polycristalline solar cells are the dominant technology on the market and represent 90% of the photovoltaic market (1). This strong increase was possible thanks to the high boost given by the public subsidies (2). However even if their price keeps lowering around 50% per year, they are not yet competitive with other energy sources. Great opportunities to continue reducing the production costs come from silicon thin film technology, while the classical silicon solar cell technology has lower margin in the future.

An alternative technology to the inorganic devices exists. Organic photovoltaic cells are devices fabricated using low cost mass production techniques, which could replace the inorganic counterpart, at least in some applications, and create new implementation of the photovoltaic technology. The discovery of conductive and semiconductive organic materials has lead to the possibility to built electronic devices with features not achievable by the inorganic counterparts. In the last 30 years, this has given rise to the development of devices such as organic batteries, organic light emitting diodes (OLEDs), organic field-effect transistor (OFETs), light emitting electrochemical cells (LECs) and organic photovoltaic cells (3) (4) (5) (6) (7) (8) . Some of these devices are already in the market or close to it, while others are still at a research stage. Organic photovoltaic cells, also known as organic solar cells, are in the latter group. Their development has increased in the last couple of years, after a previous stagnating period. Currently, organic photovoltaics (OPV) is an active field of research in which many groups participate. Several strategies are being explored in order to better understand their physical and chemical limits and to obtain reasonable power conversion efficiency. At the moment, the highest efficiency of a polymeric

solar cell at the laboratory scale is 9%, which is considered a high value compared with the standard systems, even though other technologies are already able to reach much higher efficiency, as depicted in Fig.1.1.

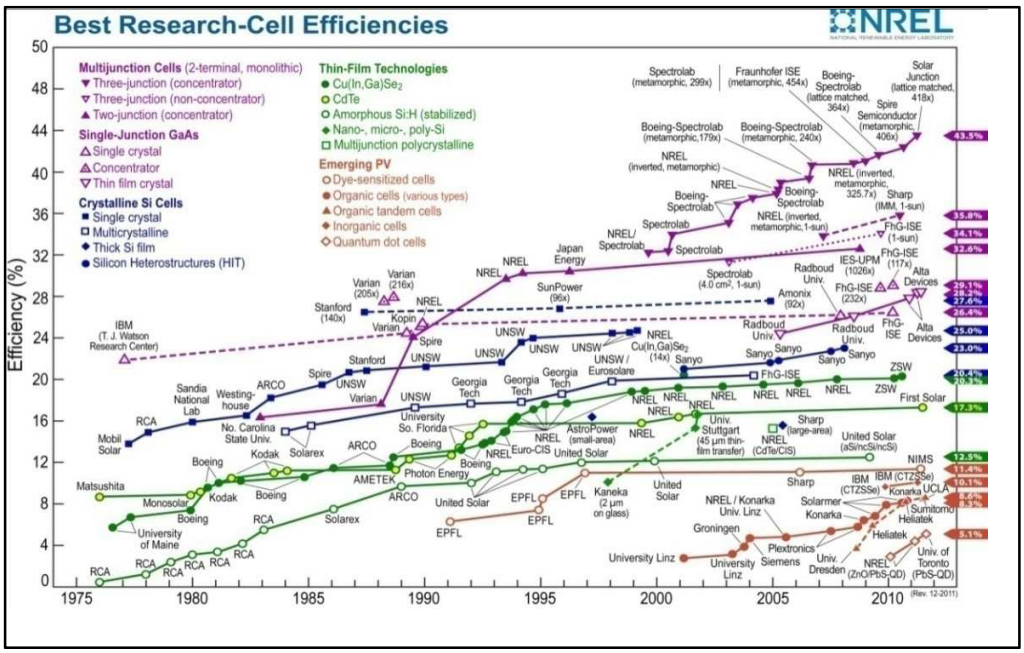

Fig.1.1 National Renewable Energy Laboratory certified efficiency of different photovoltaic technologies.

At a first glance, an organic solar cell consists of an organic active layer sandwiched between two electrodes. It is possible to distinguish between two main families of organic semiconductor materials, both based on conjugated molecules, such as cyclopentadiene and benzene rings. The first is referred to as small-molecule organic photovoltaics and the later as polymer photovoltaics.

These two new classes of materials are promising great advantages, beyond the possibilities of the standard well-developed technologies, such as:

- lower thickness
- lower weight
- flexibility (Fig.1.2)
- properties tuning by chemical tailoring

Small molecule semiconductors are not easily processed in solution due to their tendency to crystallize and in some cases due to their poor solubility. Therefore they must be processed using evaporation techniques, which complicates the production process and makes it more expensive. On the other hand, polymers are not affected by this drawback and thus polymer solar cells possess:

- easy processability on large area via wet processes, e.g. printing technology
- low cost processing technology

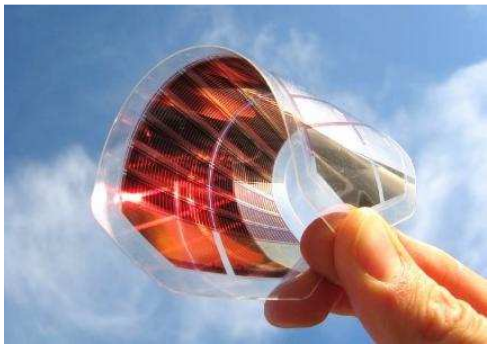

Fig.1.2 Example of the unique properties of OPV.

Besides the lower efficiency, another limiting factor of OPVs is their stability. The organic molecules, in both the classes described above, are much more prone to degradation phenomena due to the light radiation and by atmosphere components, mainly oxygen and moisture, when compared with inorganic solar cells.

Thus, an acceptable trade-off between the cell's efficiency, lifetime and cost has to be reached: a stability in excess of one year under outdoor conditions is achievable for best OPVs cell now a days (9). Surprisingly, no efficiency losses were reported.

Semiconducting behavior in organic molecules originates from the sp_2 hybridization of carbon atoms (10) and the formation of conjugated systems (11). Hybridization theory is commonly used in organic chemistry and it is able to describe in a qualitative way the bonding of atoms within a molecule. Basically, it considers the formation of hybrid molecular orbitals (e.g. allowed energy levels) from the mixing of the original atomic orbitals, superimposing them in different proportion depending on each case. The carbon sp_2 hybridization originates from the combination of the 2s and two 2 p-orbitals, leaving unchanged the last p orbital. Thus, carbon atoms in this configuration are able to use the sp_2 orbitals to form three σ bonds and the remaining p_z orbital gives rise to a regular π bond. The three σ bonds are lying in a plane, to which the π bond is perpendicular. A Schrödinger equation for the hybridized system describing the outcoming molecular orbital is a linear combination of the atomic orbitals involved. Fig.1.3 shows a representation of these concepts. The combination of orbitals from two carbon atoms permits only two solutions, e.g. the bonding and antibonding orbitals, but the interaction among several atoms produces a series of molecular orbitals which get energetically closer as the number of participating atoms increases.

These concepts are peculiar of molecular materials, but they are comparable to well-known counterpart in inorganic materials, where they are easier to explain. When a high number of atoms are forming regular inorganic

lattice, electrons are allowed to occupy levels with slightly different energy, which being present in a huge number are not discrete levels anymore, but they form continuous bands instead.

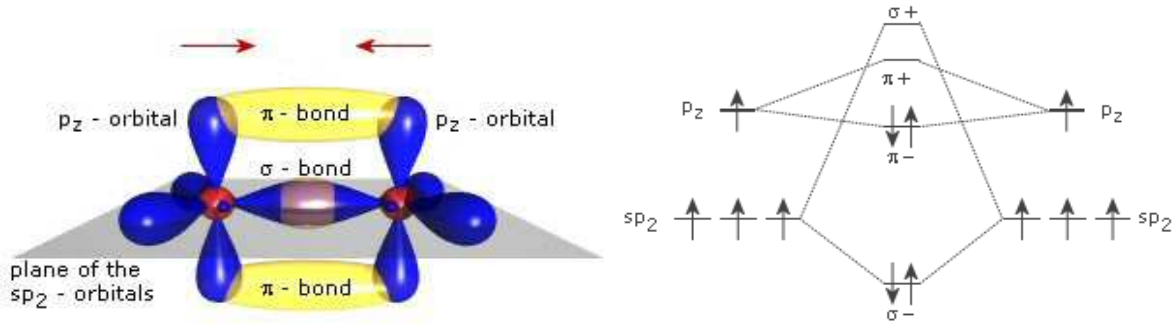

Fig.1.3 On the left, sp_2 hybridization and double bond formed between two carbon atoms. On the right, energy levels after hybridization (10).

The width of the bands depends on the orbitals from which they are formed, e.g. from the atoms present in the lattice. At 0K, the highest occupied band is called valence band (VB) while the lowest empty band is known as conductive band (CB). The minimum energy separation between these two bands, where the density of state is nil, is identified as bandgap and its width determines the conduction properties of the material. Conductors have no separation between CB and VB, while an insulator presents a large bandgap value. If the gap is not high (compared with the thermal energy kT), it is possible to promote an electron from the valence to the conduction band, using several processes. These materials are termed semiconductors.

Organic molecules do not have bands but they present instead a series of allowed energy levels. This situation gives rise to several complications when explaining their semiconducting behavior. Yet most researchers tend to use the language and concepts developed for the inorganic semiconductors field.

Concepts analogous to VB and CB are found in organics: the bonding states, with a maximum energy corresponding to the highest occupied molecular orbital, HOMO, and the antibonding states, with the lowest level being identified as lowest unoccupied molecular orbital, LUMO. The energy difference between HOMO and LUMO is termed energy gap, E_g, though some researchers tend to use the term bandgap, by similarity with the inorganic semiconductors. The energy gap of a molecule corresponds to the energy required to excite an electron from the HOMO to the LUMO. Semiconducting properties appear when the energy difference between HOMO and LUMO is low (on the order of 1 eV, as in inorganic semiconductors). In Fig.1.4 a benzene ring is shown and its structure and energy levels used as an example.

In the bonding between two sp_2 hybridized carbon atoms a σ and a π bond are formed, as shown in Fig.1.3. For the first, the energy difference between the occupied bonding orbital and the unoccupied anti-bonding orbital will lead to insulating properties, as the energy required to excite an electron is large. Instead, energy difference

between π and π* orbitals is much lower and can induce semiconducting properties and the ability to absorb light in or near the visible spectral range.

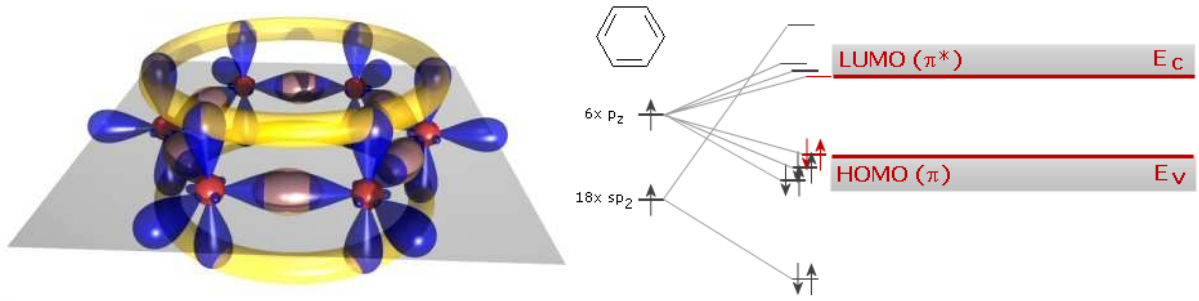

Fig.1.4 On the left, carbon-bounding structure in benzene. On the right, energy structure of a small-molecule semiconductor (10).

Benzene rings are extensively used in organic electronics, because the ensemble of π bonds is delocalized and forms a π system extending across the entire molecule. The combination of benzene and benzene-like rings, directly bounded or separated by double or triple bonds, leads to the extension of the π and π^* orbitals, up to what is known as conjugation length, leading to a decrease of the energy gap with respect to the isolated units. Thus the gap between HOMO and LUMO becomes smaller with the increase of delocalization, leading to absorption and fluorescence phenomena in the visible region of the spectrum.

In polymeric organic semiconductors, a long chain of carbon atoms constitutes the backbone, and the π system is formed along the chain, producing a one-dimensional electronic system (in Fig.1.5). Its spatial extent is limited by defects and/or disorder. The energy gap can be tuned by chemical modification of the repeat units (monomers) and by controlling the steric hindrance between them. The conduction mechanism involves charges hopping between chains or chain segments, which means that the charge transport is much more limited when comparing with inorganic crystals. It is even lower in amorphous/disordered systems. However, this is not the only critical property when it comes to conjugated polymers and oligomers applications in organic optoelectronics in general, and in particular for OPVs.

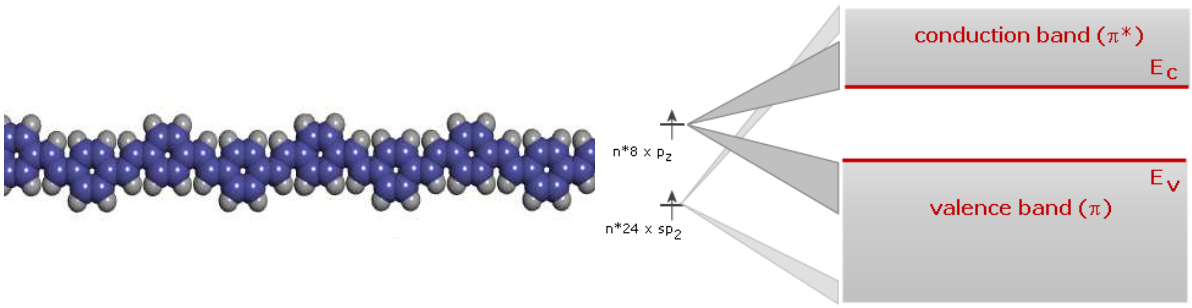

Fig.1.5 On the left, carbon-bonding structure of poly(*p*-phenylene vinylene). On the right, energy structure of a polymer organic semiconductor (10).

Device physics

The processes involved in the production of electrical current by the photovoltaic effect in organic semiconductors are not as simple, or at least, are not as well understood, as those taking place in the inorganic materials. In the next sections, the physical phenomena and the different aspects involved in the processes that leads to the production of current in OPVs are discussed. In particular, we will discuss the following four steps (Fig.1.6):

- Light absorption and exciton generation (process i)
- Exciton diffusion (process ii)
- Exciton dissociation and separation of the Coulomb-bound electron–hole pair (processes iii and iv)
- Charge transport and charge collection (processes v and vi)

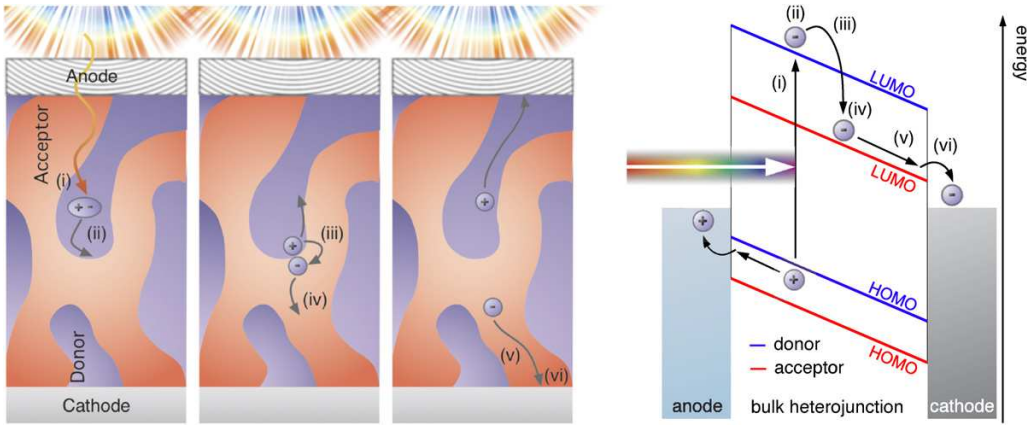

Fig.1.6 Entire photocurrent generation process. On the left, it is represented from a kinetic point of view while, on the right, a simplified energy diagram, not showing exciton binding energy (1).

Light absorption and exciton generation

In polymer-fullerene devices, which represent the most used system in polymeric solar cells, light is predominantly absorbed by the polymeric electron donor material of the heterojunction. At the moment, there are not yet well performing electron acceptors with reasonable light absorption ability. Due to the molecular arrangement and the lack of lattice effect with favourite wavevectors, an organic semiconductor has always a direct bandgap. This aspect is reflected in a higher photons absorption efficiency compared with Si or Ge semiconductors. Thus, organic materials exhibit very high absorption coefficients if compared with their inorganic counterpart, and very thin

layers are able to provide high absorption yields. The organic layer thickness commonly used is in the range of 100 to 300nm, while polycrystalline $CuInSe_2$ and Si need, respectively, less and more than hundred micrometers. On the other hand, organics present narrow absorption bands and the normally used polymers are mostly able to absorb in the visible part of the spectrum, while inorganic semiconductors absorb across large spectral ranges of the solar spectrum.

The absorption of a photon promotes an electron to a electronic excited state from which, due to the π-system relaxation ability, it reaches the lowest excited state and thus, creating a Coulomb bound electron-hole pairs. This specie is termed exciton, or Frenkel exciton, and its formation as first photogenerate specie was a question of debate for many years ((i) in Fig.1.6). Thermalization process is a significant source of power loss, especially in low energy gap materials which are designed to collect near infrared photons (12). In OPVs based on polymers combined with fullerenes, excitons are generated almost entirely in the donor materials. The exciton's binding energy is in the order of 0.5eV and it is much larger than the thermal energy contribution, which can be able to dissociate weakly bound species. This exciton binding energy can be estimated considering the interaction of an exciton as a Coulombic attraction between an electron and a hole in a material with low dielectric constant (as is the case of the organic semiconductors) at a distance of 1nm. The low dielectric constant of organic semiconductors, usually between 3 and 4, which gives a large screening length, is the final reason for direct excitons generation. Excitons usually reside in one molecule or along a polymer chain, and are thus known as intrachain excitons, even though excitons residing in close molecules were reported, and are indicated as interchain excitons. The excitons generated upon light absorption are singlet excitons, in contrast with the ones that are formed upon charge injection (in OLED, for instance) which can be singlets or triplets. Lifetime of singlet excitons is around 1 ns. After that they recombine either radiatively, through a photoluminescence mechanism, or not-radiatively. Triplets, which can be produced from singlets by intersystem crossing, are not yet advantageous and represent a loss mechanism. Fortunately, in systems with planar conformation or without heavy atoms, intersystem crossing is almost negligible.

Exciton diffusion

The simplest single layer OPV structure based on a single material is not a good approach, because it is not able to provide excitons' splitting in an efficient way. An efficient way to obtain excitons dissociation consists in the coupling of two materials with different electron affinity. Thus, after singlet excitons' generation, they have to move to an electron donor/electron acceptor interface, D/A interface, where they can fast and efficiently be dissociated upon electron transfer to the acceptor molecule ((ii) in Fig.1.6). Excitons that are generated far away

from an interface will not be able to be splitted, and will decay without generating charge. The excitons decay occurs in the timescale of pico- or nanoseconds, and is this lifetime, combined with exciton's diffusion coefficient, that determines the diffusion length:

$$L = \sqrt{D\tau} \tag{1.1}$$

where D is the diffusion coefficient and τ the exciton lifetime.

The domain size of the phases formed by the two materials has to be accurately controlled: a fine grained structure is desirable for excitons dissociation but, when the phases are getting too small, this will interfere in the subsequent steps of electron and hole transport and collection. In order to optimize the output of a cell, a trade-off between such opposite requirements has to be achieved. Organic crystals typically present exciton diffusion lengths of ca. 100nm, with important applications for bilayer planar devices, while disordered combinations of materials in blends admit much lower lengths, in the range 3 – 30 nm (1). Thus, the morphology of the active layer has a strong influence on the cell performance. Several groups have been investigating the effect of the blend details on cell performance (13) (14) (15), and theoretical models for morphology simulation were developed. Excitons, as well as charge carriers, move by a hopping mechanism in organic materials, meaning that close packed arrangements and flat molecular structures usually show better transport properties.

Exciton dissociation

The separation of an exciton is not possible by thermal energy alone, because at room temperature this energy is insufficient to overcome the exciton's binding energy. An efficient way to achieve exciton dissociation in its two charge carriers is the creation of an interface between two materials with different electron affinity, EA, and ionization potential, IP. The material with the higher electron affinity is called electron acceptor, because the electrons are moving to the LUMO of this molecule, while the semiconductor with the lower ionization potential is named electron donor, or alternatively hole acceptor, and it transports the holes at the HOMO energy level.

The dissociation mechanism is not completely understood yet. It is often described as a two step process (12). An exciton coming across a D/A interface is subjected to intermolecular charge transfer ((iii) in Fig.1.6), leading to a charge-transfer (CT) state D+/A-, where the hole resides on the donor molecule and the electron is on the acceptor molecule but the two are still Coulombically bound ((iv) in Fig.1.6). CT states have a great influence in the photocurrent generation process, due to their long lifetime and to the several processes they can undergo. In polymer-fullerene systems their lifetime is in the range 1-100 ns (16). A CT state can be subjected to dissociation, into free carriers, passing through a series of charge-separated states (CS), or undergo recombination, indicated as

geminate recombination, which can be either radiative or nonradiative. Moving through a series of CS state, e.g. hopping through molecules of donor and acceptor, the bonded electron and hole are progressively separated and become free polarons after a separation larger than the screening length is achieved. The energy of the final CS state, E_{final}, is defined as the difference of the ionization potential of the donor and the electronic affinity of the acceptor, and it represents the upper limit for the open-circuit voltage of the device. The final energy can be approximated as the difference between the HOMO level of the donor and the LUMO level of acceptor (17). This is an approximation, because the energy position of the states is not well known after the series of transfer processes. Depending of the time scale of the internal conversion, two possible paths for the exciton dissociation process can be followed, forming "hot" or "relaxed" excitons. This topic will not be discuss here, going beyond the objective of this work and is considered not to be relevant for the context of this work.

Concerning the recombination process, the transition to the ground state is the more probable event, even though back transfer of an electron from the acceptor to the donor is also possible. In the second case, regeneration of a donor singlet exciton or the transition to a triplet exciton state in the donor material are the mechanisms involved. Besides, when two oppositely charged polarons meet, a recombination process called non-geminate recombination may occur and CT states are again the intermediate states. The term non-geminate is used because the two polarons were generated independently from one another, while geminative recombination occurs between species coming from the same dissociation process.

Charge transport and charge collection

After exciton separation, free charges are present in the donor and acceptor materials and can move toward the corresponding electrode ((v) in Fig.1.6) if one of the two conditions are met:

- Diffusion of charge carriers, if electron and hole blocking layers are interposed between the active layer and the anode, and cathode respectively. The accumulation of one species of charge carriers on one side causes a gradient toward the other electrode.
- Drift of charge carriers, by using two electrodes with different workfunctions. The difference between the two energy levels is known as built-in voltage, V_{bi}, and, after the alignment of the Fermi levels subsequent to the contact between the electrodes, it acts as a driving force for the free charge carriers separation and migration.

The efficiency with which charge carriers reach the electrodes depends on their mobility. Organic semiconductors have low electrical transport ability and this results in a strong dependence of the charge carriers mobility on the active layer morphology, varying by several order of magnitude according to the degree of disorder of the materials. Amorphous films present mobilities on the order of 10^{-6} to 10^{-3} cm^2 V^{-1} s^{-1}, while highly crystalline systems can have mobilities higher than 1 cm^2 V^{-1} s^{-1}. Crystalline inorganic semiconductors present much higher mobilities values, about 10^2-10^3 cm^2 V^{-1} s^{-1}. The low mobility in the organic molecules is due to the weak electronic coupling due to the intermolecular character, structural disorder effect and the large electron-vibration coupling, leading to structural relaxation. Thus, the transport mechanism involves the formation of polarons, e.g. charges coupled to local molecular distortions, moving by hopping.

Non-geminate recombination is experimentally found to be in the microsecond to millisecond range, and considering the low mobility in organic semiconductors, the limiting step is the mutual finding of opposite charged free polarons.

The last step before having a net current flowing in the outer external circuit is the collection of the charges at the electrodes ((vi) in Fig.1.6). The process depends on the complex organic/metal electrode interfaces and the efficiency of the collection cannot be simply determined knowing the work function of the single metals, the ionization potential of the donor and the electron affinity of the acceptor. The electrode deposition process on the active layer, or vice versa, leads to several effects at the interface and the present knowledge is quite limited. Charge density redistribution, geometry modifications and chemical reactions are some of the processes that are involved, and are able to affect the position of the organic energy levels with respect to the metals Fermi level.

Device structure

The solar cell basic structure is composed by one or more active layers sandwiched between two electrodes. The light enters the device through one of the electrodes, which should be as transparent as possible, permitting the highest possible percentage of electromagnetic radiation to reach the active layer. The part of radiation that is not absorbed is normally reflected by the other electrode and passes again through the active layer. The device is fabricated on a glass or on a plastic substrate, which provides the physical support of the cell. Glass does not present mechanical flexibility, nullifying one of the advantages deriving from the use of the organic semiconductors technology. In order to obtain flexible devices, the next development steps will be to move to

polymeric substrate and produce the multilayer structure using printing techniques. This requires the researches to reconsider some aspects in the device structure, for example the use of ITO because it presents a resistivity 3 times higher, about 60 Ω/Sq, on plastic substrate compared with the one on glass.

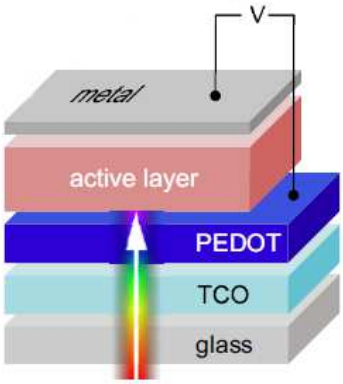

Fig.1.7 General structure of an organic solar cell (modified from (1)).

The *active layer* is fabricated on top of the anode and is responsible for the absorption of sunlight, the separation of charges and their transport to the electrodes. Along the years, two main architectures were developed for organic photovoltaic cells technology. Organic molecules present higher absorption coefficients than the inorganic counterpart, making possible to obtain high absorption of the incident light with much lower thicknesses. The usual thickness of the active layer is around hundreds of nanometer. As describe above, due to the molecular nature of OPVs and to their low dielectric constant, excitons are the primary species to be generated upon light absorption. An interface between a donor and an acceptor is needed, and thus, the active layer must contain two kinds of molecules with different electron affinity properties. The diffusion length of the exciton depends on the molecule structure: its order of magnitude is around 10 nm and this is an important parameter to be taken into consideration if we aim to achieve efficient current generation.

The extraction of the holes is carried out by the *anode* of the cell. It is usually constituted by a Indium Tin Oxide (ITO) film, deposited by sputtering on the glass substrate, covered by a Poly(3,4-ethylenedioxythiophene) poly(styrenesulfonate) (PEDOT:PSS) layer.

ITO is a transparent conductive oxide, TCO, made of a solid state solution of 90% In_2O_3 and 10% SnO_2. It is a well-known inorganic transparent conducting film (TCF), permitting the light to pass through it and creating one of the electrodes for carriers extraction. It has a work function of -4.7 eV. It is used in the electronic devices due to its transparency in thin film condition and its good conductivity. A trade-off between these two properties has to be

found, being both depending on the thickness of the layer: an increase of the thickness leads to an increase of conductivity, but decreases its transparency. A thickness of 150 nm is normally used. Its roughness is around 2 nm (rms value).

The high conductivity of ITO is related to the presence of shallow donor state located close to the host indium oxide conducting band or to the presence of oxygen vacancy states in In_2O_3 (18). The substitutional doping of Sn^{4+} in the host lattice creates a singly charged donor state, due to Sn higher valence compared to In. At room temperature, electrons of the donor states undergo thermal ionization into the host conductive band. At higher doping level, discrete levels form an impurity band and electrons density in the conducting band leads to a condition of degenerate gas of electrons, such as the model normally used to describe conduction in metals. The oxygen vacancies creation provides electrons by acting as doubly charged donors. Each oxygen vacancy is surrounded by In^{3+} 5s orbitals, which are stabilized from the In 5s conduction band by a lack of covalent bonding with the missing O^{2-}. Thus, In 5s orbitals form a shallow donor state just below the edge of the conduction band, that is able to trap two electrons, at every oxygen vacancy site. At high concentration value of vacancies, the discrete levels form a band which again overlaps the conduction one.

The energetic level arrangement explains ITO's high electronic conductivity and its far infrared absorption, leaving unchanged the fundamental bandgap of the host oxide and thus, maintaining the transparent feature of the material.

PEDOT:PSS is a mixture of two polymers: the conjugated polymer poly(3,4-ethylenedioxythiohene) and polystyrene sulfonic acid, which acts as a dopant, and is available as an aqueous dispersion. It is used to fabricate conductive transparent thin films. It also creates a perfectly flat anode surface, smoothing the irregularity of ITO surface. PEDOT has good electrochemical and thermal stability and the electrical properties typical of the polythiophenes family. It is necessary to mix PEDOT with PSS in order to improve its solubility and stability, as otherwise it would not disperse in water and would suffer fast oxidation in air. The polymerization degree of PEDOT is limited to about 20 monomeric units. PSS increases its processability, acting as a counter ion, which disperse PEDOT chains in the solvent. PEDOT:PSS has a work function of -5.2 eV.

Another interesting class of materials, whose presence is getting usual in organic photovoltaic cells and in other organic electronic devices, are the transition-metal oxides. Due to wide spread in their chemical, physical and electrical properties, these materials are good candidates as electrodes, permitting the tuning of the electron injection/extraction properties. The more investigated hole-injecting oxides are MoO_3, WO_3, V_2O_5, CuO and NiO, while TiO_2 and ZrO_2 are well-known electron-injectors. They can be produced by thermal evaporation as well as by solution processes. Their work function and the electronic structure can be easily tuned by inducing defects or changing their oxidation state. Greiner at al. (19) proved that the driving force for energy levels alignment is electrochemical potential thus, due to the wide range in their work function, metal oxides can be made to obtain

work functions that are close in energy to the HOMO and LUMO of the organic semiconductors and permit a good charge extraction.

The *cathode* is made of a metal with low work function (WF), or a series of metals layers, evaporated after the active layer production. The role of the cathode is to collect the electrons produced upon excitons dissociation: in order to have efficient collection, the cathode must present a work function level lower than the LUMO of the electron transporting materials. The cathode materials usually used in polymeric solar cells are aluminum, Al, or silver, Ag, with a thickness of ca. 70 nm. In a short-circuit condition, the Fermi levels of the electrodes must align or otherwise a net current will pass through the device. The alignment of the Fermi levels of electrode causes the bending, or better, a tilting in the energy levels of the semiconductors materials and this is the main driving force responsible for the collection of the generated charge carriers to the correct electrode. Concentration of charges close to the interface is also producing a drift, but its effect is smaller compared with the previous one and not able to provide good device efficiency. In order to obtain efficient charges collection, it is required to couple electrodes with large difference in work function, because this will lead to stronger tilting. Al and Ag do not have such large difference with PEDOT:PSS work function, thus a thin interlayer can be added, such as 5nm of lithium fluoride, LiF, or barium, Ba, as they have much lower work function values. LiF also produces an interfacial dipole, which is basically lowering the work function of the cathode and making the collection process even more efficient. It was also reported that the interlayer of LiF avoids damages of the active layer due to the incident hot metal atoms, enhances the fill factor and stabilizes high open circuit voltages (20).

The material used as electrode strongly influences cell performance, as it determines the type of contact that is created (Ohmic or Schottky barrier contact). If a Schottky contact is formed, the experimental V_{oc} is in agreement with the MIM model and its value is the difference between the work functions of the electrodes. In case of an Ohmic contact, V_{oc} is determined by the difference between the LUMO energy of the acceptor and the HOMO level of the donor.

The production of the cathode electrode using evaporation techniques is a crucial issue. The metal evaporation is a time demanding operation, because it requires the evaporation chamber to be under vacuum. Besides, it limits the possibility to produce low cost devices on a large scale, reducing one of the benefits of organic solar cells.

Active layer architecture

The particular mechanism of charge carriers generation in organic semiconductors imposes the need to develop more complex active layer architecture when comparing with the ones used in inorganic photovoltaic devices.

The first efficient active layer architecture was developed by Tang in the '80s (21) and was named *planar bilayers heterojunction* (see Fig.1.8, on the right). It consists in a two separated layers of organic materials, with different electron affinity and ionization potential, fabricated one above the other by evaporation or by wet process. The contact area between the donor and the acceptor material is equal to the area of the cell. This leads to the fact that only the excitons produced by the absorption of light at a distance smaller than their diffusion length from the planar interface can be split. It is not able to efficiently produce free charge carriers, because in the greater part of the device the excitons decay to the ground state without generating charge. On the other hand, bilayer structure ensures a good collection of the charge carriers to the correct electrode, reducing free charges recombination. Now a days, bilayer devices are not able to reach high efficiency values and their strength can only be exploited as long as the exciton diffusion length is longer than the absorption length. The bilayer architecture is usually made with high absorbing dyes as electron donors and buckminsterfullerene, C_{60}, or its derivates, as electron acceptor, which are usually evaporated.

In the early '90s, a different architecture, called *bulk heterojunction* (Fig.1.8, on the left), was developed and it is the one used in this work (22) (23). Here, the two organic semiconductors are mixed in solution forming a blend, and the film is produced by a coating technique. Another possibility, in order to obtain a bulk heterojunction, is to co-evaporate the two materials. The intimate mixing of donor and acceptor material gives rise to a larger interface, making the excitons separation not the limiting issue. Having an interface present throughout all the cell's thickness, this architecture is able to efficiently produce free charge carriers and thus higher conversion efficiency values are achieved when compared with the bilayer structure. On the opposite side, the charge extraction by the right electrode gets more difficult and recombination becomes a more important issue.

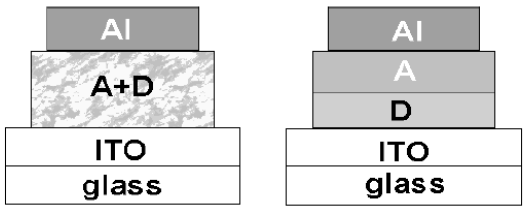

Fig.1.8 Bulk heterojunction and planar bilayer heterojunction, respectively, on the left and on the right (24).

Another possible architecture, known as *laminated device*, was proposed. It should create a compromise solution combining advantages of the bilayer and of the bulk heterojunction architectures. A single layer of donor and acceptor are prepared on two different substrates, which are heated and then the organic surfaces are joint together, creating some intermixing in the contact zone. In this way, and at the same time, the recombination should be more limited than in the bulk heterojunction and the excitons separation is more probable than in a bilayer cell. This approach is not common yet, mainly because it requires specific properties of the organic semiconductors, for example the glass transition temperature, T_g, of the two components in order to obtain adhesion and strength after the junction process.

A further improvement, coming from the inorganic semiconductors' world and which some groups successfully realized also with organic materials, is the introduction of the *p-i-n structure*. The idea is to produce a series of stacked layers which have different carriers transport properties, through a process of doping. The process of doping can be obtained in several ways, for example co-evaporating molecules with high holes or electrons transport properties, respectively with the donor or acceptor. Differently from inorganic, the concept of enhancing the ability of a layer to transport just one kind of charge carrier through a doping process is not crucial in organic materials (25). The reason is their own ability to transport electrons and holes, according to the molecular structure of each molecule, and, for a long time, doping was not used due to the difficulty to produce stable and reproducible doped organic layers. Several improvements were obtained in the last decade, as published by Drechsel at al. (26). This approach was already used in fabrication of pin-type OLED, demonstrating high efficiency even at high brightness.

According to the function carried out by the electrodes, the final created structure is:

- a highly doped material with hole transporting ability, indicated as p-doped, in contact with the anode of the cell
- an intrinsic layer in the middle, without a net doping effect which is responsible for light absorption
- a highly doped material with electrons transporting ability, indicated as n-doped, in contact with the cathode of the cell

The implementation of the p-i-n structure in a photovoltaic device presents several advantages compared with the condition of direct contact of the active layer with the electrodes:

- recombination at the electrodes is avoided, being not possible for excitons and minority carriers to move through the doped materials.
- the absorbing layer thickness can be optimized, reduced as much as needed, in order to have better quantum efficiency, preventing recombination at the metallic contact, and preventing problems of shorts between the electrodes, because the overall electric field is redistributed on the total thickness, thus, also in the doped zones.
- It is possible to tune the position of the different layers according to the internal distribution of the electrical field of the radiation.

On the other hand, one possible drawback of a p-i-n structure, in which the same materials are used for p, i and n layer, is the possibility of exciton quenching in the doped zones which may compete with the charge separation. This phenomenon observed in OLED, is expected to be longer than the excitons dissociation kinetics in organic photovoltaic devices and thus should not have a significant influence. Further studies are obviously required in this area.

This structure was already successfully produced by co-evaporating molecules with dopant agents (26). The p-i-n formed in this way is fixed, and its realization required several evaporations. Further improvement is the realization of a dynamic p-i-n structure by in situ electrochemical doping as shown by Heeger and co-workers (27). They showed the possibility to obtain a doping effect by the movement of ions presents in the active layer, drifted by an external applied bias. This concept was already used in the production of light emitting devices, where the spatial separation of ions accompanying the oxidation or reduction of the active materials at the electrodes is one of the proposed working mechanism of light-emitting electrochemical cells (LECs). The main advantages introduced by this technology compared with OLEDs are the possibility to use air stable electrodes, a complete solution based process and a simpler structure, where the several layers of OLED are substituted by a single layer carrying out several function.

Polymeric solar cells with dynamic p-i-n structure have also been demonstrated (28). Su et al. prepared a bulk heterojunction of MEH-PPV/PCBM OPV adding polyethylene oxide (PEO) and metal triflate salts. MEH-PPV/PCBM is a donor/acceptor system commonly used in the past, to which they add PEO in order to provide a solid-state solvent for the ions movement. Obviously, the addition of PEO produced an important initial decrease in the device performance because it does not have an active role in photon absorption or current transport. The salts used are composed by a triflate anion ($CF_3SO_3^-$) and an inorganic metal cation, such as Li^+, K^+, Ca^{2+}, Zn^{2+}. In the published work it was possible to obtain an increase of the PCE from 10 to 40%.

This thesis reports the endeavors to achieve a p-i-n structure in a P3HT:PCBM system, where a small amount of ionic liquid was added to the blend, aiming to achieve higher power conversion efficiency, PCE.

Chapter 2 -
Electrical characterization of a solar cell

The characterization of an electrical component is obtained measuring the value of an output parameter at different values of the input one. The most common used pair of parameters are the current (I), or current density (J), and the voltage (V). An organic photovoltaic cell, being essentially a diode, is characterized by an asymmetric IV curve, known as the characteristic curve of the device. For practical use, and in order to facilitate device comparison, it is more adequate to work with the current density, even though we will continue to indicate it as IV curve.

The IV curve of a non illuminated device has the shape of a regular diode characterization curve, obviously with the parameters peculiar to the organic material used. In the case of reverse bias, a very small current is present, known as the leakage current. Moving toward positive bias, thus in a condition of forward bias, in the beginning no current will flow through the device. The flow of charges starts only after a threshold value, which is one of the parameters that characterizes the diode. When an illumination source irradiates the semiconductor material, an additional current due to the photoelectric effect flows through the device:

$$J = J_0 + J_{ph} \tag{2.1}$$

where J is the total current density, J_0 is the current flowing through the diode due to the external voltage source and J_{ph} is the photogenerated current. This produces a shift of the IV curve towards the third and fourth quadrants. The photogenerated current has a negative value, which simply means that it has negative direction considering the current convention normally used in electronics. Fig.2.1 shows an example of an IV curve of an organic solar cell.

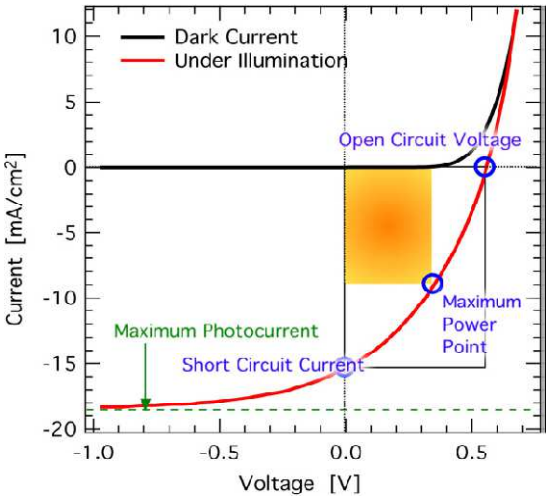

Fig.2.1 An example of the IV characterization curve for an OPV cell (1).

In an IV curve, it is possible to recognize two points which represent important features of the device:

- the open circuit voltage, V_{oc}, which is the maximum drop of voltage created between the electrodes of the cell. It corresponds to the maximum energy of the charge carriers that are extracted from the device and enter into the external circuit
- the short-circuit current, I_{sc}, corresponding to the maximum current passing through the electrodes if an ideal connection is realized between them

In a first approximation, it is possible to consider that V_{oc} depends on the work function of the electrodes and on the energy levels of the organic semiconductors.

The short circuit current depends on the amount of radiation absorbed, i.e., on the overlapping of the absorption spectrum of the organic material with the irradiated solar spectrum. The absorption is a function of the absorption coefficient of the material, which is wavelength dependent, and on the thickness of the layer. The absorption of a photon is able to promote an electron from its ground state to an excited one, only if its energy is at least as large as the energy separation between the two states. This wavelength is known as critical wavelength, and it is a characteristic parameter of the used semiconductor. The maximum I_{sc} producible can be calculated considering the material's absorption, and calculating the number of absorbed photons which is, in principle, equal to the number of electrons excited from the ground state

$$P_{abs}(\lambda) = \frac{h\,c}{\lambda}\, n_{phot} \tag{2.2}$$

Thus,

$$n_{phot} = P_{abs}(\lambda)\frac{\lambda}{h\,c} \tag{2.3}$$

Where n_{phot} is the number of absorbed photons per unit time and unit area, P_{abs} is the absorbed electromagnetic power at each wavelength, h is the Planck's constant, c the speed of light in vacuum and λ the wavelength of the radiation. Integrating the number of absorbed photons up to the critical wavelength value, and multiplying with the elementary charge, the theoretical value of the I_{sc} can be obtained. A solar cell is subjected to a large amount of loss processes, and the current normally has lower values than the theoretical one.

Another important parameter to characterize the device performance is the maximum power point (MP or P_{max}), which is the maximum of the product of current and voltage, I_{mp} and V_{mp}. This is the most important parameter in terms of electrical performance since it gives us the maximum electrical power that our device can produce. When the cell is connected to an external circuit, the equivalent external load resistance sets the voltage at which the cell is working, thus the amount of current that is possible to extract. The optimal value of the equivalent resistance is obtainable by the equation

$$R = \frac{V_{mp}}{I_{mp}} \tag{2.4}$$

For all other load resistance values, the OPV will be working in conditions away from the maximum power point and thus, loosing produced power.

The maximum power produced is higher as much as I_{mp} and V_{mp} approach, respectively, the values of I_{sc} and V_{oc}. A figure of merit in order to quantify this aspect is the fill factor, FF, which measures the ratio between the produced power and the theoretical maximum producible power. In a graphical representation, it is the area of the rectangle having vertexes in the axes origin and in MP, while the theoretical maximum is the product of the short circuit current times the open circuit voltage.

$$FF = \frac{I_{mp}V_{mp}}{I_{sc}V_{oc}} = \frac{P_{max}}{I_{sc}V_{oc}} \tag{2.5}$$

Or equivalently rewritten as

$$P_{max} = V_{oc}\,I_{sc}\,FF \tag{2.6}$$

There are several loss processes happening inside the cell, which lead to a reduction of the produced power from the theoretical value. Losses are due to recombination processes at the different steps of the production and extraction of charge carriers from the device, and can be divided in:

- exciton decay before it reaches an interface
- geminate recombination, or recombination of the interfacial charge transfer states
- non-geminate recombination, or recombination of the free charges after exciton dissociation
- charge extraction losses at the electrode interfaces

The importance of these processes depends on the system used, and is strongly dependent on the morphology of the active layer. The control of the morphology is clearly one of the most important variables that must be addressed when optimizing devices performance.

Knowing the incoming power into the cell, it is possible to calculate the efficiency of the electromagnetic radiation to electrical power conversion process. The power conversion efficiency PCE, or η, is defined as the ratio between the outcoming electrical power over the incoming solar power

$$\eta = \frac{V_{oc}\, I_{sc}\, FF}{P_{light}} \tag{2.7}$$

Some of the above mentioned parameters are wavelength, spectral distribution and light intensity dependent. Therefore, it is important to consider standard conditions in order to compare the conversion efficiency of cells. Solar radiation standards were defined and must be used in order to obtain a standard characterization of a photovoltaic device. AM0 is the solar spectrum outside Earth atmosphere, while the most common AM1.5 is the standard spectrum at sea level. If a G letter is present, that means that it corresponds to the global spectrum, containing all the physical phenomena at which light is subjected in the atmosphere (refraction, reflection, scattering, etc…). The AM1.5 Global spectrum has a total power of 1000 W/m^2 (100 mW/cm^2).

In order to produce high electrical power, large values of both V_{oc} and I_{sc} are required. The energy gap between the ground and the excited state is an important figure of merit. Large V_{oc} values are obtained for large gaps, but this leads to a narrowing of absorbed light wavelength range. Thus, more photons with lower energy are lost. On the other hand, more electrons can be promoted with low energy gap materials, but the maximum V_{oc} will be smaller. A trade-off between these two parameters is needed, in order to obtain the highest power production. The highest efficiency is reached with semiconductors with energy gap between 1.1eV and 1.5eV. In inorganic semiconductor, Shokley and Quessier were the first to propose a model considering this double influence of the energy gap. Besides, they also considered all the possible loss mechanisms and calculated a maximum efficiency value of 30%. This value is even lower in organic solar cell, due to the exciton binding energy and other restrictions on V_{oc}. Obviously, V_{oc} cannot be higher than the difference between the LUMO of the acceptor and the HOMO of the donor. Scharber at al. (17) developed a thumb-rule for the determination of the open circuit voltage, after testing many blends of PCBM and different polymeric donors. The result was a linear relationship:

$$V_{oc} = \left(\frac{1}{e}\right)\left(|HOMO_{Donor}| - |LUMO_{PCBM}|\right) - 0.3 \tag{2.8}$$

where the energy values of HOMO and LUMO are in eV, and e is the elementary charge. The value of 0.3V is an empirical factor and it is valid only if the HOMO of the donor and the LUMO of the acceptor are aligned with the respective electrodes. On the other cases, this experimental value is even larger and consequently V_{oc} is smaller. The selection of the electrodes has a direct influence on the output of the cell and the best results are obtained with Ca and Au (29) (30). The low work function of Ca is an advantage for the type of contact created but leads to a higher instability towards oxidation, while Au has to be very thin in order to be transparent. Besides, a difference of approximately 0.5eV between the LUMO of the donor and the LUMO of the acceptor is required in order to achieve an efficient exciton dissociation at the D/A interface.

Another useful parameter to characterize a cell is the external quantum efficiency, EQE. For each wavelength, it measures the fraction of incident photons that are converted into electrons able to pass to the external circuit. EQE plots provide information about the ability of the material to absorb the incident photons and on the efficiency in the extraction of the charge carriers produced, at each wavelength.

A solar cell, such as any electrical devices, can be described as a network of ideal electrical components. This representation is called equivalent circuit diagram, ECD, and it is a powerful tool able to describe a physical phenomenon as the behavior of one or a group of ideal components. In this way, it is possible to model the behavior of a cell, determine its parameters and try to understand the occurring loss processes. The basic ECD of a photovoltaic cell is shown in Fig.2.2.

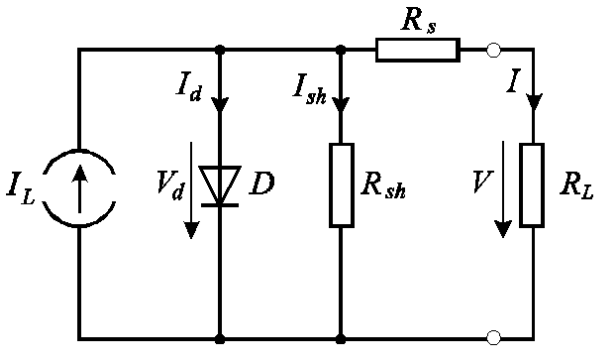

Fig.2.2 Basic ECD of a photovoltaic cell (24).

I_L represents the ideal current source due to the light illumination and R_L is the load resistor. The ideal diode, D, models the nonlinear shape of the characteristic IV curve. It determines the current flow from the anode to the cathode and not on the opposite direction, or rectification, due to the difference between the HOMO of the donor and the LUMO of the acceptor or due to the blocking contact for electrons at anode and for holes at the cathode. The IV curve is determined just by the diode behavior only if R_s=0 Ω and R_{sh}=∞ Ω. The ideal current source, I_{ph}, represents the photocurrent generated under illumination, before any recombination process takes place. The

series resistor R_s, considers the mobility of the charge carriers in the respective transport material. The mobility depends on the transport mechanism, which is hopping in organic materials, and is affected by space charges, traps and long travelling distances of the charges, e.g. thicker transport layers. It is estimated from the reverse of the slope of the curve at $V>V_{oc}$ because, at these voltages, the diode conducts and R_s dominates the behavior of the curve. The shunt resistor, R_{sh}, is due to recombination of charge carriers at the D/A interface and usually also near the electrodes. It can be derived considering the reverse slope of the IV curve at 0V.

This circuit is valid for inorganic, as well as, for organic semiconductors. In addition, the ECD for organic devices can include another diode and two capacitors C_μ and C_g. The second diode takes into account the formation of blocking contact at the extracting electrode for both charge carriers, which can lead to FF<0.25 in the IV curve. The geometrical capacitor, C_g, considers charge/discharging effects, due to the time that charge carriers need to travel along materials with low conductivity, such as the organic semiconductors. The chemical capacitor, C_μ, is due to the different transport ability of materials, and considers charge accumulation at the interface between them (31).

Considering the presented elements, it is possible to derive equations describing the short-circuit current, the open circuit voltage and the produced power of our device. The mathematic description of the device goes beyond the aim of this work, and the presented concepts will be used just to understand the processes involved in the OPVs operation after the production of a p-i-n structure.

Chapter 3 - Materials

Introduction

The nature of the donor and acceptor materials plays an essential role in the performance of a solar cell. The final performance depends on the properties of the materials themselves, e.g. their absorption coefficient or their energy band gap, as well as on the combination of their properties, such as the relative position of the energy levels. Larger device efficiencies are always related with the development in materials science, even though new molecules design is not the only direction to follow in order to obtain improvements of devices performance. Important aspects to be investigated are also the chemical compatibility between donor and acceptor, their ratio, the solvent and the structure of the produced phases. All these aspects influence the photocurrent generation and extraction, and studies regarding these parameters are required in order to optimized the devices. One of the most used material blend is the mixture of poly(3-hexylthiophene) and [6,6]-phenyl-C61 butyric acid methylester, P3HT:PCBM. This is the system used in this work, but it will be modified by the addition of an ionic liquid.

P3HT:PCBM

One of the most used polymeric donor material is regioregular poly(3-hexylthiophene), RR P3HT, depicted in Fig.3.1 on the right. It presents reasonable environmental stability, high hole mobility and improved absorption compared to poly(*p*-phenylene vinylene)s, which were used in the previous generation of devices. The materials with the best acceptor properties are buckminster fullerenes, C_{60}, and its derivates. The most used fullerene is

[6,6]-phenyl-C61 butyric acid methylester, PCBM, depicted in Fig.3.1 on the left. The large use of PCBM is due to its solubility in organic solvents, while C_{60} has to be evaporated. Their good acceptor characteristics are probably the result of the combination of spherical shape and the favorable electron affinity. The main disadvantages of PCBM are its rather low absorption in the visible spectrum and its cost, which represents almost 10% of the entire device cost (32). Using P3HT:PCBM blend, the highest efficiency reached was about 5% after active layer morphology optimization. Several new materials were reported in the last decade, able to reach efficiencies even higher than 9%. The key issues of polymer design include engineering the bandgap and energy levels, in order to achieve high I_{sc} and V_{oc}, enhancing planarity to attain high carrier mobility, and materials processability and stability. P3HT has a HOMO level at -5.1eV, which, using equation 2.1, corresponds to a V_{oc} of around 0.6V and it is used as reference in polymer design. The HOMO level of polymers can be lowered, leading to a V_{oc} increase, if electron poor groups are used for instance. By incorporating fluorene and carbazole units into a polymer donor, V_{oc} is significantly increased. On the other hand, a common strategy in order to increase I_{sc} is to design materials with lower bandgap, which permits a larger coverage of the solar spectrum (33). The efficiency of the P3HT:PCBM system is strongly dependent on the morphology of the film, which can be tuned according to the processing conditions. Considering that P3HT presents an exciton diffusion length of 4nm (1), this determines the ideal size of the nanoscale phase separation in the active layer in order to lower excitons' recombination. Photoluminescence in P3HT is weak, and the surplus energy after recombination is converted to heat.

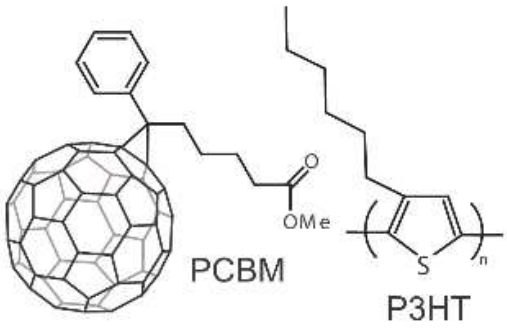

Fig.3.1 PCBM structure on the left, P3HT structure on the right.

Regioregularity, RR, refers to the arrangement of monomers in a head-to-tail configuration along the polymer chain instead of head-to-head. It was proved that optical and transport properties of P3HT increase with increasing regioregularity degree (34). Best device performance was reported using a donor with the highest available regioregularity (95.4%). RR P3HT tends to form planar structures, known as lamellae, which are normal to the substrate surface and this gives rise to strong interchain interactions. An increase in the absorption coefficient of P3HT, with a red-shifted absorption shoulder at 600 nm, and a larger field-effect mobility were observed. The self-

organized RR P3HT structure is observed also in the presence of PCBM, in devices with ratio 1:1 by weight. A thermal treatment, described below, can enhance even more this molecular ordering.

The crystalline fraction of P3HT in the blend has a strong effect on the device performance and that can be tuned using different processes. A controlled thermal treatment, normally called annealing, increases the crystalline fraction and thus improves cell performance. Cells based on non-annealed P3HT:PCBM show efficiencies than can be lower by one order of magnitude. The treatment is performed at an optimum temperature on the order of hundred Celsius degrees, and then cooled down to room temperature, producing the reorientation of the chains and the formation of crystalline domains. The controlled crystallization produces an increase in hole mobility and a red shifting of the optical absorption of P3HT, producing a better overlapping with the solar spectrum (35). The increase in the hole mobility in P3HT can achieve three orders of magnitude and is able to give rise to a I_{sc} five times higher than the one in the as-cast device. In the latter, the difference between hole mobility and electron mobility is much too large and the photocurrent is limited by the formation of a space-charge condition. After annealing the difference is reduced to a factor of 20: electron mobility is around $2*10^{-7}$ $m^2V^{-1}s^{-1}$, while the hole mobility was measured to be 10^{-8} $m^2V^{-1}s^{-1}$. The red shift (with the presence of a strong absorption peak around 510 nm, depending on the annealing temperature) may be attributed to an increased interchain interaction among P3HT molecules, resulting in a more delocalized conjugated π electrons and the lowering of the bandgap. Excess annealing leads to larger P3HT domains, and subsequently to a decrease in performance. This is one of the degradation mechanisms.

The thermal treatment effect on the morphology can also be recognized in the variation of the surface roughness, specified by the root mean square, rms, values. In Tab.3.1 a brief comparison of its values taken from Li et al. (36) is shown.

Tab.3.1 Effect of annealing on the rms roughness of P3HT:PCBM.

Thermal treatment temperature for 20 min [°C]	Rms [nm]
As-cast	0.377
70	0.662
110	0.91
150	0.75

In literature, there are some discrepancies when specifying the best heat treatment to be performed. Temperature and time affect in slightly different way I_{sc}, FF and PCE (36). Good results were reported for treatment at 150°C for 5 min or at 135°C for 20 min.

In the fabrication sequence, annealing can be performed before or after the cathode deposition and that represents another variable to consider. Surprisingly, better performances are obtained if the thermal treatment is

done after cathode deposition. The phenomenon was explained considering that the metal cathode acts as a vertical barrier, reducing the possibility of vertical movements of the chains and instead enhancing chains orientation in the plane, thus, leading to improved transport ability of the materials. Padinger at al. reported on the combined effect of an annealing treatment associated with the application of an external voltage higher than V_{oc} to the device. Comparing with the effect of annealing alone, a further increase of the performance was reported. This was explained with an enhancement of the orientation of the chains due to the electric field applied between the electrodes (37).

The thickness of the active layer has an important influence on the performance of the cell. Thinner devices are not able to provide a good photon harvesting, while they guarantee an efficient charge collection to the electrodes. Thicker devices suffer from an increase in recombination losses but are more efficient in solar energy absorption.

The solvent plays an important role in the performance of the cell. Some studies showed an influence of the concentration of the solution of the blend in the performance of the cell (38). Better performances were reported with a concentration of 70 mg/ml on P3HT:PCBM system with composition 1:0.8 by weight. The choice of the solvent is another factor that influences the final morphology of the active layer, also in terms of stability. Commonly used solvents for P3HT:PCBM blends are chlorobenzene, CB, and orto-dichlorobenzene, ODCB. From both solvents, it was reported the formation of PCBM clusters in the active layer after thermal treatment, which are larger in the case of ODCB (39). This experimental evidence was explained considering that ODCB has a higher boiling point than CB, and thus, more solvent molecules remain trapped inside the bulk heterojunction layer. Due to the solvent traces, PCBM is easily able to diffuse inside the polymer matrix and form larger agglomerates, increasing the phase separation and thus reducing the (local) power conversion efficiency of the device. High boiling point solvents, evaporating slowly, allow a better crystallization.

It was also reported that, even after evaporation of the solvent molecules, the active layer is able to capture back solvent molecules from the surrounding environment. It is possible to improve the solvent elimination introducing a high convective air flow during the thermal treatment. This implies that the morphology of the active layer is influenced also from the solvent pressure in the atmosphere, and not only by the solvent used for the casting. The influence of the local solvent atmosphere may contribute to explain the different results obtained from different laboratories or in different days in the same glove box. In literature, no works regarding the solvent content after a vacuum treatments, as the one at which devices are subjected during the cathode deposition, were found. Vacuum and thermal treatment could play a synergic effect on the morphology of the film. Additives can be used in order to decrease the diffusion rate of PCBM and to improve the stability of the bulk heterojunction

morphology: nitrobenzene is able to suppress the PCBM diffusion, while 1-chloronaphthalene or 1,8-diiodooctane enhance this phenomenon (39).

Ionic liquid

In order to achieve the aim of creating a dynamic p-i-n structure, we added an ionic liquid, IL, to the standard blend P3HT:PCBM dissolved in clorobenzene. As a general definition, an ionic liquid is a salt with a melting point below room temperature or below an arbitrary temperature. While liquids are composed by neutral species, IL are made of ions. Ionic liquids have been used in a wide range of applications, such as solvents, electrically conductive fluids, quenching media, heat transfer and storage media in solar thermal energy systems and many others. A much larger range of applications was possible with the introduction of ionic liquids with weakly coordinating anions (anions that interact only weakly with cations) such as hexafluorophosphate (PF_6^-) and tetrafluoroborate (BF_4^-), by Wilkes and Zawarotko in 1992 (40).

Ionic liquids have several useful features if compared with the inorganic salts:

- Soluble in most organic solvents and insoluble in water
- Chemically and electrochemically stable at temperatures lower than 200°C and within large potential range
- High ionic conductivity reaching 0.1 S cm^{-1}

The high ionic conductivity combined with the high stability promote the application of ionic liquids in electrochemical devices. They were already used in LECs technology, in order to build a p-i-n structure able to provide favorable features to this device (41).

Imidazolium salts are especially appreciated for the large tunable chemical structure and polarity. This should permit to blend ILs directly with conjugated polymers, without need of additional electrolyte in the fabrication. In our case, we studied two ionic liquids, 1-butyl-3-methylimidazolium hexafluorophosphate and tetra-n-butylammonium tetraphenylborate, whose structures are reported in Fig.3.2 and some properties in Tab.3.2

Tab.3.2 Some properties of the ionic liquid used in this work.

	1-butyl-3-methylimidazolium hexafluorophosphate	tetra-n-butylammonium tetraphenylborate
Provider	Sigma-Aldrich®	Sigma-Aldrich®
Melting point	6.5°C	230°C
Boiling point	>340°C	-
Density (at 20°C)	1.38 g/ml	-
Molecular weight	284.18	561.69

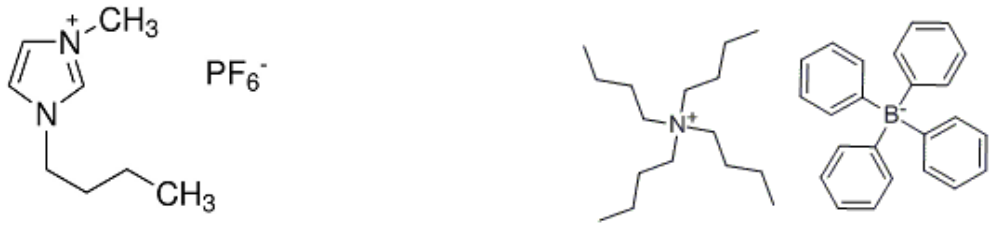

Fig.3.2 1-butyl-3-methylimidazolium hexafluorophosphate structure on the left, and tetra-n-butylammonium tetraphenylborate structure on the right.

Chapter 4 -
Equipment and Methods

Introduction

In this chapter a description of the processes and conditions used to produce the devices are reported. The devices were produced at ICMol (Instituto de Ciencia Molecular) laboratories of Universitat de València in Paterna. The devices were fabricated in a class 10000 clean room where plastic electronic devices, such as organic photovoltaic cells, LECs and OLEDs, are prepared. Working with thin films, a dust free and temperature controlled environment is essential in order to guarantee the reproducibility of the devices characteristics and flawless electronic characterization. The temperature is kept constant at 23°C. The entrance is allowed only wearing cleanroom suits and gloves. The clean room is protected from UV radiation coming from normal illumination in order to protect sensitive materials during the production process. A MBRAUN inert gas glove box allowed the manipulation of oxygen and moisture sensitive materials, reducing the degradation phenomena and permitting the storage of devices for longer time.

Used materials and blend preparation

The device structure is built on a borosilicate glass substrate with a thickness of 1mm, which presents a roughness of 2nm of rms value. The choice of glass is due to its transparency on the VIS-IR radiation, its chemical stability and

its good strength. It is also able to absorb most of infrared radiation above 2µm and thus reducing the heating of the active layer of the cell. On the top of the glass is deposited the ITO, described above.

The devices were prepared using commercially available materials. P3HT used was produced by Rieke Metals Inc®. at electronic grade, while Solenne [60]PCBM at 99.5% was used as acceptor. 1-butyl-3-methylimidazolium hexafluorophosphate and tetra-n-butylammonium tetraphenylborate were both obtained from Sigma-Aldrich®.

The ratio P3HT:PCBM is 1:0.8, with a blend concentration of 36mg/ml in chlorobenzene. The quantity of ionic liquid added is reported as a percentage in mass with respect to that of P3HT. The solution was mixed in a magnetic stirrer for at least 36h at room temperature. PEDOT:PSS used in device fabrication was Clevios™ P VP AI 4083.

Substrate cleaning process

Initial substrate conditions were the ones indicated by the company that supplied the ITO-coated glass substrate Several ITO patterns were available and each substrate has a pattern for the fabrication of 4 cells. According to the specific need, different patterns were used and Tab.4.1 reports the area of the final fabricated cells for each pattern. A cleaning procedure is needed, in order to remove particles, dust and organic residues from the surface, which affect in a dreadful way the device performance. The cleaning process consists in a first cleaning with soap and water, followed by a series of sonication processes in normal water, distilled water and isopropyl alcohol. Finally, a 30 minutes treatment under a UV lamp is performed.

Tab.4.1 Active area of the cells in the different available patterns.

Pattern	Cell 1 [m^2]	Cell 2 [m^2]	Cell 3 [m^2]	Cell 4 [m^2]
1	$9.0*10^{-6}$	$1.5*10^{-5}$	$3.5*10^{-5}$	$9.5*10^{-5}$
2	$6.5*10^{-6}$	$6.5*10^{-6}$	$6.5*10^{-6}$	$6.5*10^{-6}$
3	$1.2*10^{-5}$	$1.2*10^{-5}$	$1.2*10^{-5}$	$1.2*10^{-5}$

Layers spin coating

A SUSS Delta80 RC spin coater was used to fabricate the PEDOT:PSS anode layer, as well as the active layer. SUSS Delta80 RC spin coater is a semi-automatic system to produce thin films by spinning of the material solution. It is programmable with several spinning recipes, each composed by several steps, and it is possible to set the acceleration, the rotational speed and the time of the step. The coater has an automatic lid, closing the spinning work space. This feature is used to create a solvent-saturated atmosphere when high vapor pressure solvents are used, in order to prevent a fast solvent evaporation, giving non uniformity of the layer. All the process is made under a fume hood, using chlorobenzene which presents moderate toxicity.

PEDOT:PSS is taken with a syringe, and after passing throw a filter, a drop is placed on the ITO surface of the device. The spinning process has two steps, without closing the lid, and the fabrication parameters are summarized in Tab.4.2. The substrate is then subjected to a thermal treatment at 150°C for 10 minutes on a hot plate, in order to permit water evaporation. The produced PEDOT:PSS layer has a thickness of 70 nm.

Tab.4.2 Parameters used in the set up of the SUSS Delta80 RC for PEDOT:PSS layer deposition.

Step	Rotational speed [rpm]	Acceleration [rpm/s]	Time [s]
1	300	300	5
2	1000	700	30

The active layer is produced on top of the PEDOT:PSS layer. The blend solution is filtered, and a drop placed on top of the PEDOT:PSS covered substrate. The coating is performed closing the lid, and the standard parameters used are listed in Tab.4.3. The set of parameters used is not always the same, because they influence the final film thickness and we intend to investigate the effect of the thickness on the PCE.

Tab.4.3 Parameters used in the set up of the SUSS Delta80 RC for a 120 nm active layer deposition.

Step	Rotational speed [rpm]	Acceleration [rpm/s]	Time [s]
1	300	300	5
2	2000	1000	20

Cathode deposition

After the active layer fabrication, the device is placed inside an inert gas glove box. The deposition of the cathode is done using an Edwards Auto 500 thermal evaporation system.

The vacuum chamber is installed inside the glove box and it is able to achieve a pressure of the order of 10^{-6} mbar, using a rotative vane pump in series with a turbomolecular pump. Fig.4.1 shows the system diagram. The rotative vane pump starts to depressurize the chamber, and it is the only pump working till the pressure reaches 10^{-1} mbar. At that pressure level, the turbomolecular pump is turned on. The rotative vane pump continues to work at the output of the turbomolecular in order to maintain the required vacuum level. Required vacuum level is achieved in about 10 min.

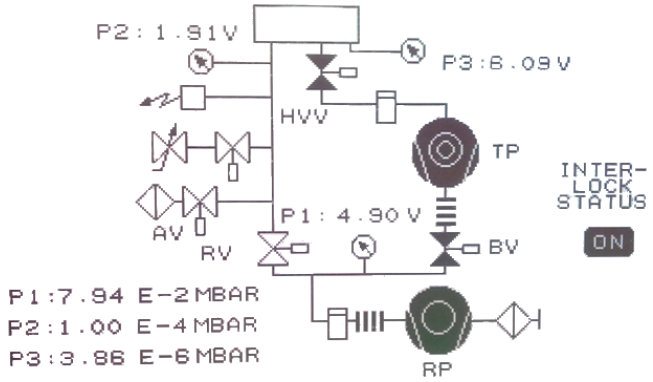

Fig.4.1 Pumping system connects with the thermal evaporation system.

The devices support is a physical shadow mask, which permits to deposit the cathode. The use of a hard mask is a very efficient fabrication technique in this case, permitting an easy and fast process. The support is rotating, in order to guarantee an homogeneous and more controlled deposition process. A shutter is present in order to protect the devices and prevent the metal deposition till the correct deposition conditions are reached.

A crystal sensor, composed by a crystal holder, a quartz crystal and a oscillator unit, with a FTM7 Film Thickness Monitor, were used to measure the deposition rate and the film thickness by a microbalance technique. The FTM7 samples the output of the oscillator unit and detects frequency changes caused by material being deposited on the surface of the crystal. The FTM7 uses the change in frequency to calculate the rate and thickness of the material being deposited.

The crucibles are fixed to metal terminals, and thus, connected to an external power circuit. When the circuit is closed, a current passes through the circuit and is able to heat the material in the crucible. A current of several ampere is normally needed to obtain evaporation. Crucibles can have different form and made of different materials, according to the material to evaporate. Typical evaporated metals are Al, Ba, Ag, Au, Ca, as well as other compounds, such as MoO_3, LiF or Cs_2Co_3. It is important that, at the working temperature, there are no reactions between the material of the crucible and the material to evaporate. According to the evaporated metal different

speed and different vacuum levels are required. A pressure around $3.7*10^{-6}$ mbar is normally used as starting point for deposition. Deposition rate depends on the materials and conditions: a rate of 0.20 Å/s for Ba and for the first 5nm of Ag or Al is used. Later, deposition rate of 1 Å/s can be used. A constant deposition rate is desirable in order to obtain homogeneous deposition, even though it is not easily achieved, especially for aluminum. The variation in the metal evaporation rate are due to changes in the physical state of the material, which changes its conductivity, and to the position of the material on the crucible. Typical deposited thicknesses and speeds for the cathodes used are reported in Tab.4.4.

Tab.4.4 Thicknesses and deposition rates of the cathodes.

Cathode material	Thickness [nm]	Deposition rate [Å/s]
Ba	5	0.20
Ag	5+65	0.20+1
Al	5+65	0.20+1

Annealing process

Annealing is extremely important for the performance of P3HT:PCBM devices, and the two main parameters affecting the final result are temperature and time. Other factors, such as the atmosphere should be investigated but they were not considered here. Annealing is performed by heating the device on a hot plate for a variable time. The effect of the thermal treatment on the P3HT:PCBM blends with ionic liquid was not known, thus different conditions were tested. At the end, the best results were obtained with the parameters contained in Tab.4.5.

Tab.4.5 Time and temperature used in the annealing process.

Annealing process	Temperature [°C]	time [min]
1	150	5
2	135	20

The annealing process can be performed before or after the cathode deposition, and this affect the final result. To perform the annealing before the cathode deposition, the devices were heated on a hot plate inside a fume hood. This condition of annealing will be referred as *pre-treatment*. On the other hand, an annealing process performed in the glove box after the cathode fabrication is referred as *post-production*. The two treatments differ not only for the presence of the second electrode (it affects the chains mobility, but also reaction and diffusion phenomena of metals atoms in the active layer could happen), but also for the different atmosphere and its solvent content. The last markedly affects the performance, and further studies should be conducted.

Device measurement

Electrical measurements of the devices were performed inside an inert gas glove box under a solar simulator from ECN (Energy research Centre of the Netherlands), which permits to obtained the characteristic IV curve of the cell under illumination and in the dark. The system also permits to apply a constant bias, before the application of the voltage sweep, in order to provide the driving force for the ions migration.

Illumination is obtained by an halogen lamp, which needs about 10 minutes to give a constant light intensity. The measure of EQE required a previous calibration step, performed with a certified reference silicon cell, in order to determine the photons emission of the lamp at each wavelengths. The EQE measurement is obtained interposing several interference filters, and recording the extracted current. Fig.4.2 shows an example of the overlap between the solar spectrum and the lamp emission. IV curve of the solar cells are recorder using a Keithley 2400 SourceMeter.

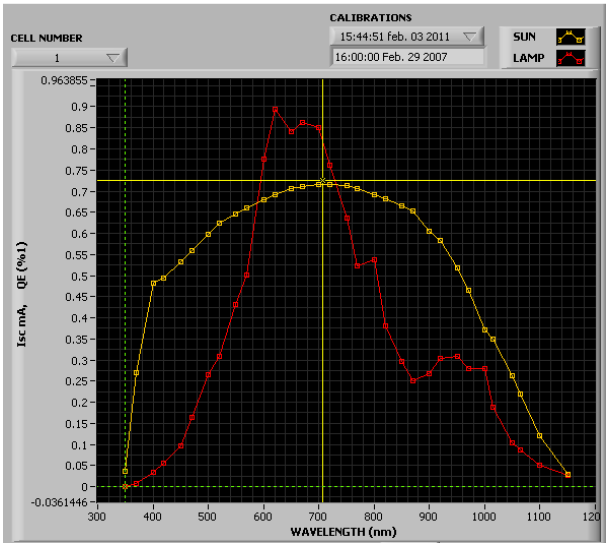

Fig.4.2 Example of the overlap between the sun spectrum and the spectrum of the lamp used for the characterization.

A specific software was used to control the calibration and the measurement operation. A different software controls the bias of the cells along the time, permitting to set the time and the constant voltage value for the bias. It also permits to set the measuring voltage ramp, according to the need. When long time bias was performed, the

cell was maintained in the dark before measuring the sweep. This prevents additional effects of heating or electric conduction, which could influence the ions movement.

Others measurements performed on our sample were:

- Absorbance measurement using a Avaspec-2048 Avantes spectrophotometer;
- Thickness measurement with an Ambios-Technology profilometer model XP-1, placed on a vibration isolation table, with an accuracy of 10nm;
- AFM measurements in tapping mode with a Veeco Nanoscope IVa Multimode Scanning Probe Microscope. Analysis of the AFM raw data was performed with WSxM software (42).

Chapter 5 -
Results and Discussion

The fabrication procedure and the environmental conditions affect the cells performance. V_{oc}, I_{sc}, FF and PCE are parameters that characterize different aspects of the cell performance. Here we have used PCE to discriminate the "best cell", being the power production the main purpose of these devices. Fig.5.1 shows the characteristic curve of the reference device P3HT:PCBM, and Tab.5.1 contains its relevant parameters. These are standard values for a P3HT:PCBM device, indicating that our experimental conditions are good. In the next discussion, the blend containing 1-butyl-3-methylimidazolium hexafluorophosphate is identified as P3HT:PCBM:mIm, and the blend containing tetra-n-butylammonium tetraphenylborate is identified as P3HT:PCBM:bAm. The quantity of IL added to the blend is referred as the percentage of its mass with respect to the mass of P3HT.

The following topics were studied:

1. Influence of ionic liquid addition on blend morphology
2. Effect of IL addition on cell performance
3. Effect of biasing the cell and formation of the p-i-n structure
4. Light intensity influence on cell performance
5. Optimization

The first issue to be discussed is the formation of the p-i-n structure. Obviously, this is not an easy task and we tried to collect data that allow us to conclude about the p-i-n formation. The approach used was to test OPVs with and without the ionic liquid under several conditions. No direct measurement of ions localization or displacement

was made. In order to evaluate cell's behavior, it is important to distinguish between the different device conditions:

- the cell after production (including annealing), indicated as *fresh cell,*
- the cell after the application of a short bias, usually 2 minutes,
- the cell after the application of a long bias, in the time scale of hours. In this case, the biasing of the cell is performed in the dark, in order to prevent temperature influence or any other possible variation of the current in time due to light exposure.

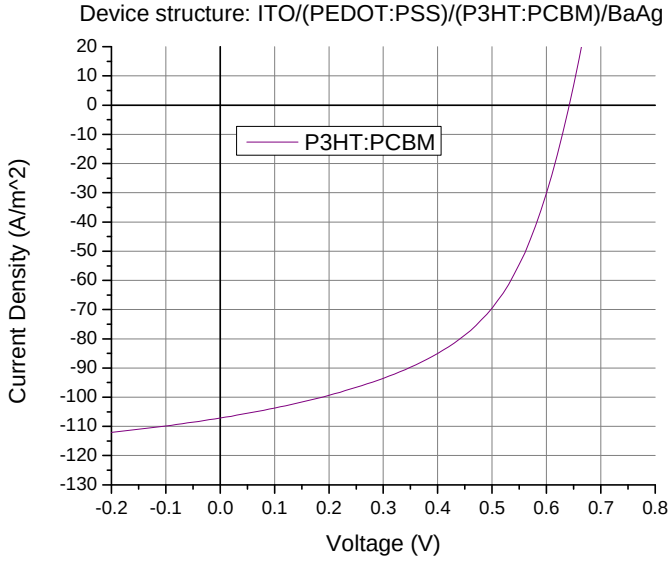

Fig.5.1 IV curve of a standard P3HT:PCBM cell.

Tab.5.1 Parameters of the P3HT:PCBM cell, whose characteristic are shown above.

	V_{oc} [mV]	I_{sc} [A m^{-2}]	FF [%]	η
P3HT:PCBM	642	-107	52	3.55

Thickness [nm]	T annealing [°C]	t annealing [min]
130	135	20

Influence of ionic liquid addition on blend morphology

In order to test the IL effect on the morphology of the blend, a series of AFM measurements were performed and compared. Fig5.2, Fig.5.3, Fig5.4, Fig.5.5 and Fig.5.6 contain the graphical representation of the AFM topography measurements, obtained on a 5 µm x 5 µm area in tapping mode. AFM samples were cut out from glass support

after preparation and an annealing treatment at 150°C for 5 min was performed in all the samples. Tab.5.2 contains the rms values obtained from the AFM measurements. The rms value of the P3HT:PCBM was taken from Li et al (36).

Analyzing the AFM results, and the extracted values in Tab.5.2, it is evident that pure PCBM is much flatter than P3HT. The addition of 5% of 1-butyl-3-methylimidazolium hexafluorophosphate does not affect PCBM morphology while, oppositely, the addition to P3HT gives rise to the formation of high and isolated peaks. These experimental results seem to indicate a better chemical compatibility of the IL with PCBM than with P3HT. The effect of addition of 5% of 1-butyl-3-methylimidazolium hexafluorophosphate on the P3HT:PCBM blend is quite strong too. High peaks surrounded by flat regions can be observed, see Fig.5.6, and an almost 6 times larger rms value was measured. The observed change in morphology should have a great impact on cell performance and affect the movement of excitons, of free polarons and maybe also of ions. We could not obtain information about ions distribution, and thus this aspect will be not considered. The contact area with the cathode is also dependent on the surface profile, increasing with the increase of the roughness.

Particularly interesting is to evaluate if the observed behavior is dependent on the nature of the ionic liquid. An opening study on this was performed, and a device with 1% of tetra-n-butylammonium tetraphenylborate was tested. Fig.5.7 contains the surface profile of this blend. Tetra-n-butylammonium tetraphenylborate seems to show smaller surface changes, which actually does not mean that it has less influence on the overall morphology. A single peak was registered, probably due to dust or other kind of particle, which slightly increase the rms value. Anyway, the rms value is quite close to that of P3HT:PCBM. Tetra-n-butylammonium tetraphenylborate seems to be much more compatible with P3HT, even though the concentration of IL was different in the two cases. Previous study on PPV:PCBM and metal triflate salts (28) shows changes in morphology of the film after the application of a bias. This we did not determine.

Tab.5.2 Roughness rms values extracted from AFM measurements in several blends.

	Rms value [nm]
P3HT	1.25
P3HT:5%mIm	6.53
PCBM	0.54
PCBM:5%mIm	0.52
P3HT:PCBM	0.75 (Ref. (36))
P3HT:PCBM:5%mIm	4.38
P3HT:PCBM:1%bAm	0.94

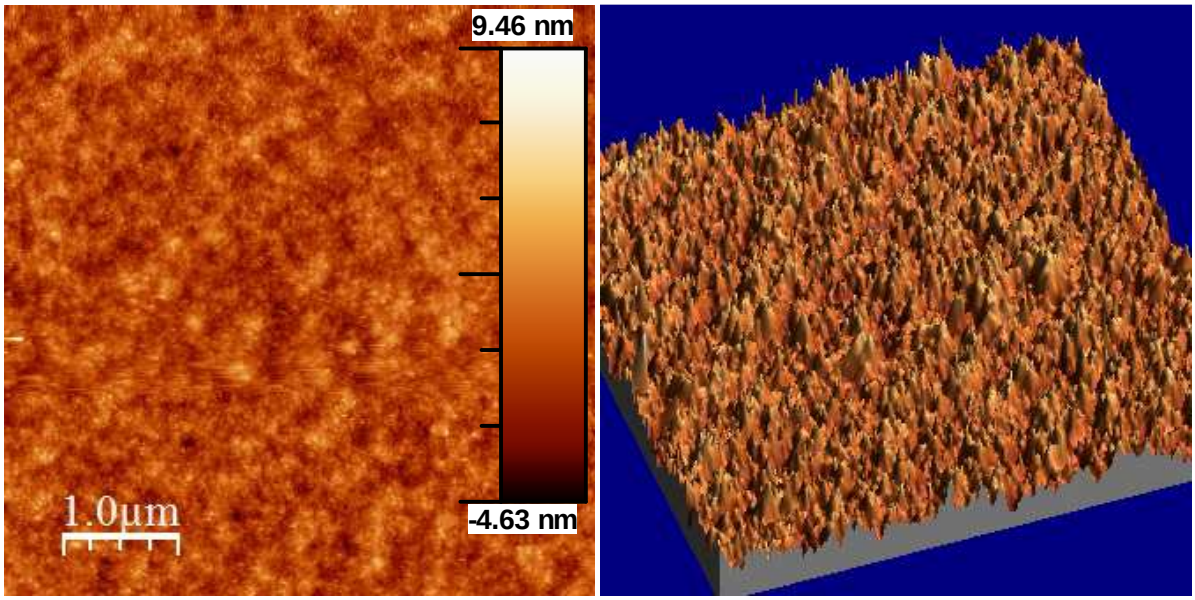

Fig.5.2 P3HT AFM topography measurement. 2D representation on the left, and 3D reconstruction on the right.

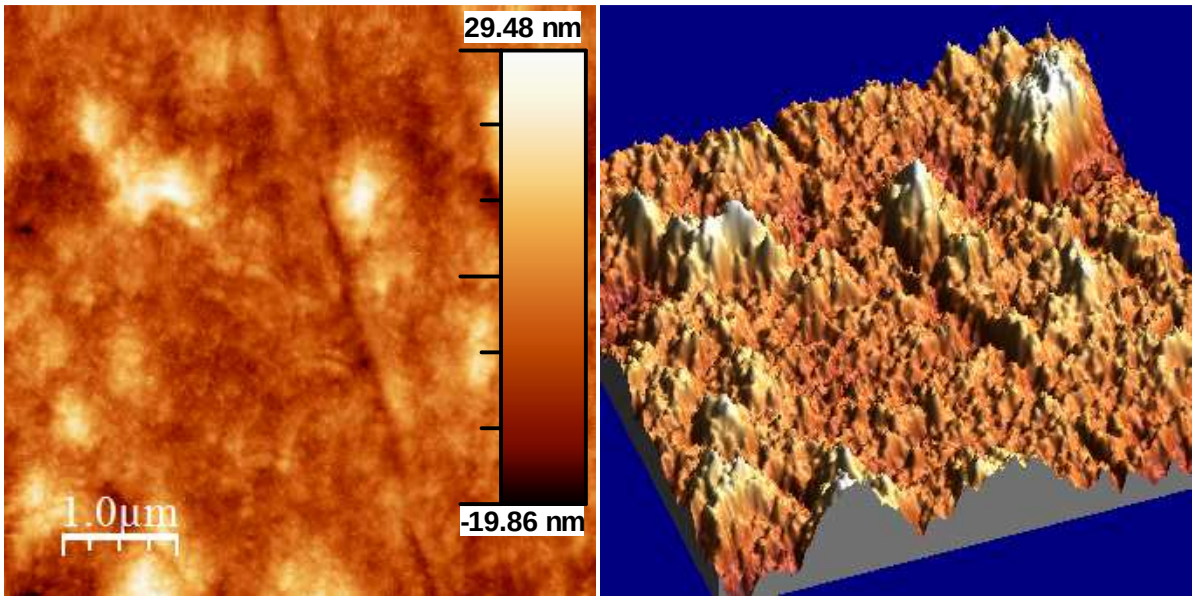

Fig.5.3 P3HT:5%mIm AFM topography measurement. 2D representation on the left, and 3D reconstruction on the right.

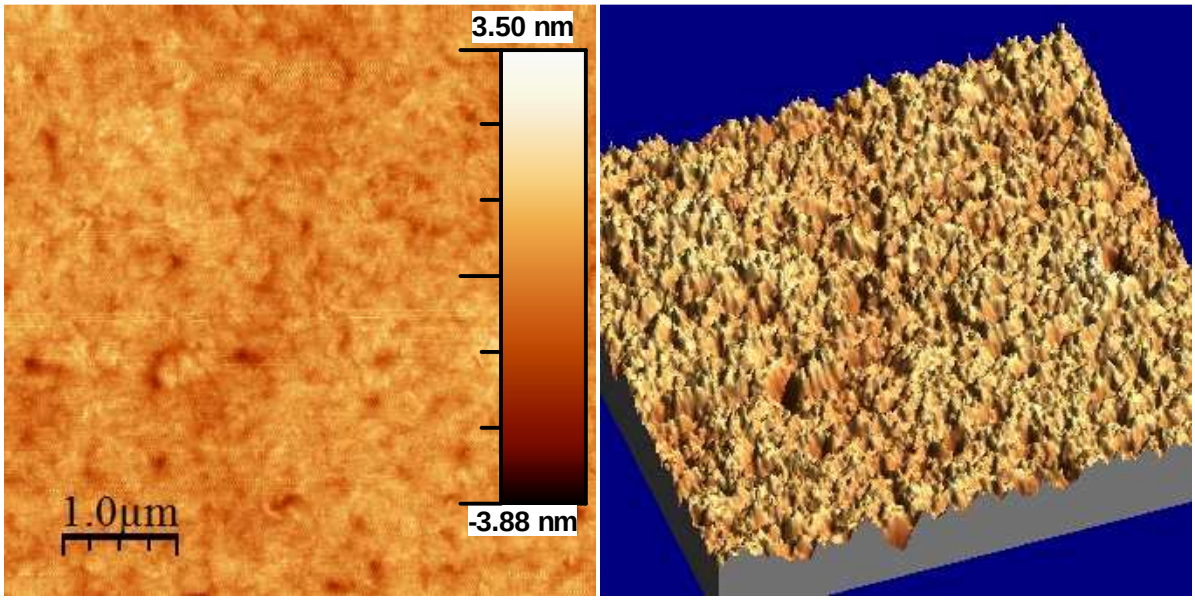

Fig.5.4 PCBM AFM topography measurement. 2D representation on the left, and 3D reconstruction on the right.

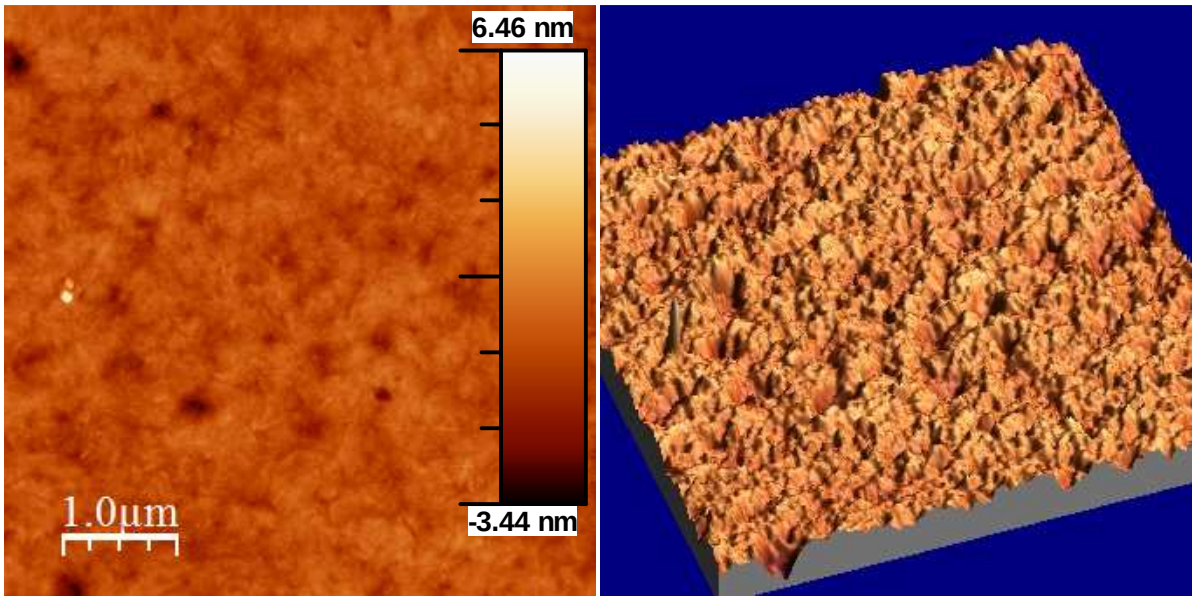

Fig.5.5 PCBM:5%mIm AFM topography measurement. 2D representation on the left, and 3D reconstruction on the right.

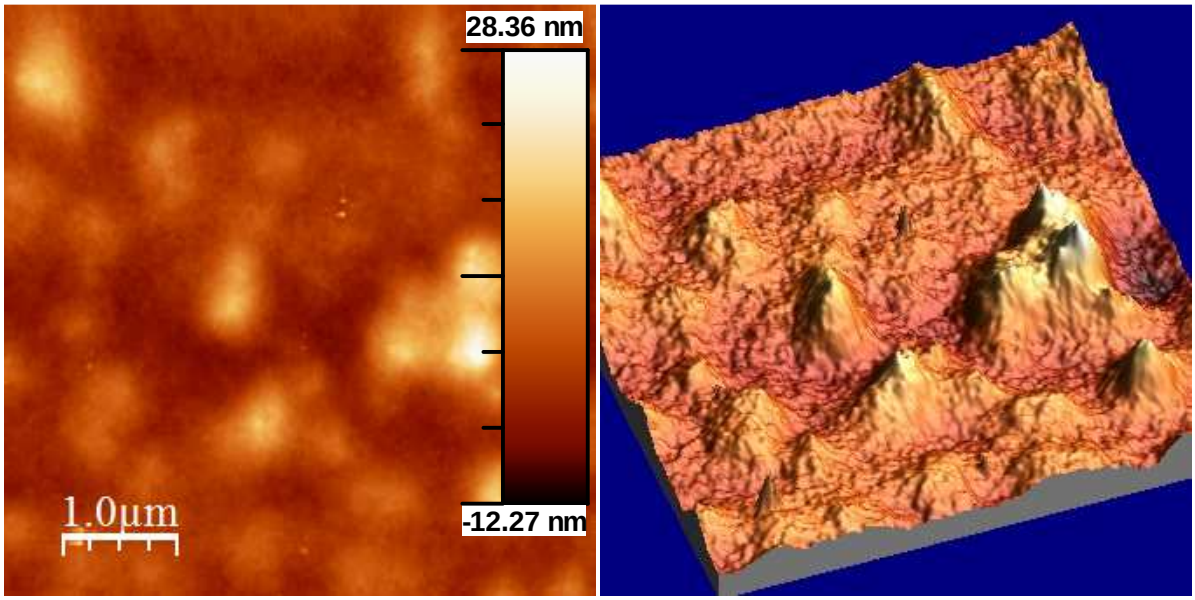

Fig.5.6 P3HT:PCBM:5%mIm AFM topography measurement. 2D representation on the left, and 3D reconstruction on the right.

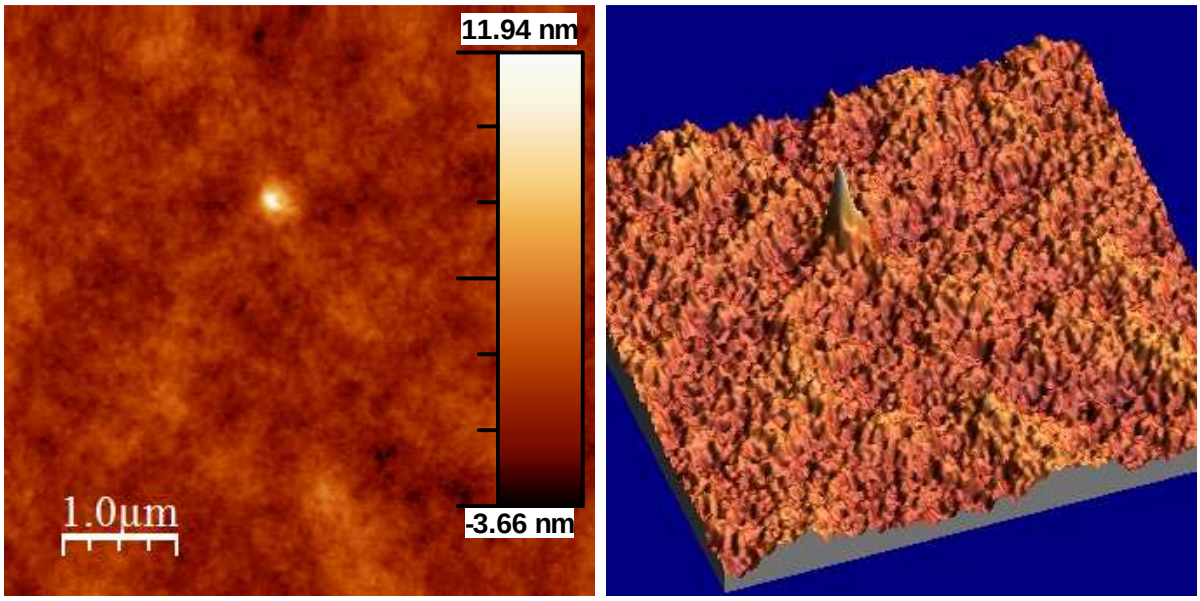

Fig.5.7 P3HT:PCBM:1%bAm AFM topography measurement. 2D representation on the left, and 3D reconstruction on the right.

Effect of IL addition on cell performance

Fig.5.8 shows a typical IV curve of a fresh device based on P3HT:PCBM:5%mIm, and in Tab.5.3 its parameters. Active layer thickness, IL concentration, choice of IL to add, etc, are parameters that strongly influence device performance. Considering the complexity of the studied situation, here a simple description of the common features of devices containing or not an IL is presented. In the Optimization section, a further analysis of several parameters is reported. Here, in order to be more representative, average curves were calculated from the four cells present on each substrate.

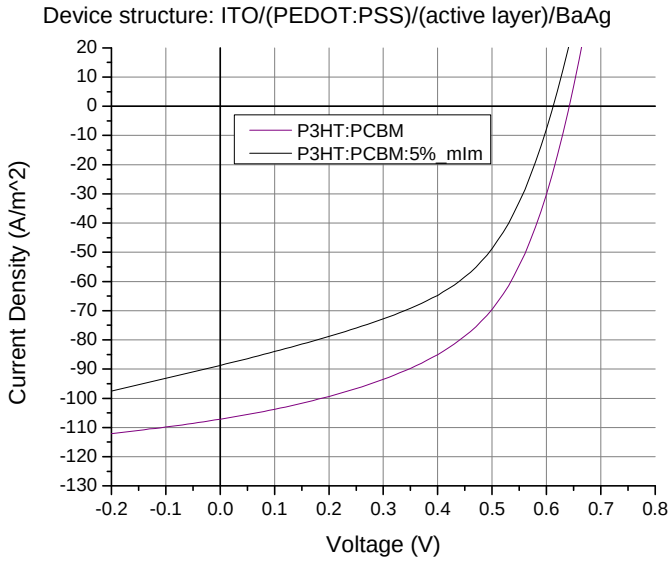

Fig.5.8 IV curves of a P3HT:PCBM:5%mIm and a P3HT:PCBM cell.

Tab.5.3 Parameters of fresh P3HT:PCBM:5%mIm cell.

	V_{oc} [mV]	I_{sc} [A m^{-2}]	FF [%]	η
P3HT:PCBM:5%mIm	618	-89	48	2.64

Thickness [nm]	T annealing [°C]	t annealing [min]
190	135	20

The addition of IL decreases the device power conversion efficiency, accompanied by a reduction of all the important device parameters. The IL containing device shown above has a higher thickness than the P3HT:PCBM used as reference, but the performance reduction was verified to be a common feature in all the produced cells. The reason for the reduction on V_{oc}, by about 20 mV, is not immediately clear, and further studies are required. The reduction of the current density can be partially explained by a reduction in the absorption of the incident light due to the addition of IL, which is not absorbing. Obviously, this phenomenon should get more important increasing the IL concentration. The variation of absorption is evident in Fig.5.9 by plotting the absorbance versus

wavelength of a standard blend and of a blend with 5% of 1-butyl-3-methylimidazolium hexafluorophosphate. For the same thickness, around 120 nm, a slight reduction in the absorption spectrum is reported, with a decrease of the absorption peaks of P3HT at 520 nm and of PCBM at 330 nm.

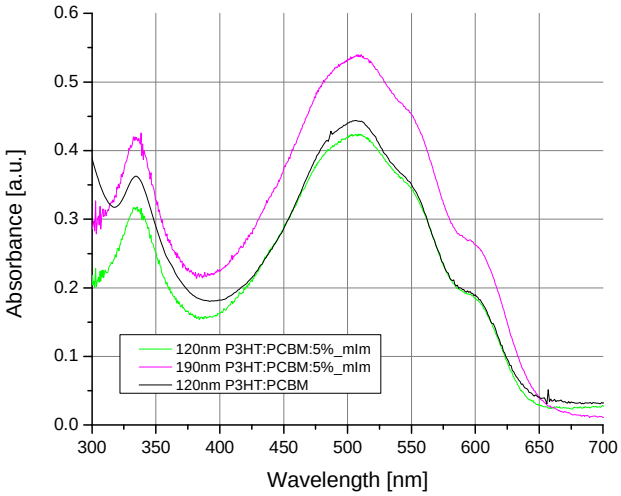

Fig.5.9 Comparison of the absorption spectra of P3HT:PCBM and P3HT:PCBM:5%mIm.

Besides the reduced absorption, IL addition changes the morphology of the active layer and this could negatively affect the cell: a wrong morphology induces strong recombination phenomena, which leads to lower PCE. For the P3HT:PCBM:5%mIm system, the device performance was better when a film thickness of 190 nm was used. In contrast, in the laboratory where this study was done, the best performance for the P3HT:PCBM system was obtained with an active layer thickness of 120 nm.

Annealing of the layers is an efficient way to increase the PCE of P3HT:PCBM devices, but it could induce some unexpected and/or undesired effect after addition of the IL. The annealing at 135°C for 20 minutes or at 150°C for 5 minutes, which gave the best PCE in the standard system, leads also to an increase in performance for the IL containing devices, even though no information about ions movement influence was obtained.

An issue that was not investigated is the application of a bias to a system incorporating ions during the annealing process. Interesting effects might appear when biasing at different temperatures, considering that temperature affects the movement of ions, as well as of electrons.

Similarly to the results reported for the standard system, we observed that in blends with ionic liquid, the pre-treatment gives rise to a better PCE than a post-treatment.

Effect of biasing of the cell and formation of the p-i-n structure

The following step in the study of the cells was the application of a constant voltage, referred to as bias, for 2 minutes prior to the cell characterization. In a first approach, a negative bias was applied first, followed by a positive bias. The characterization curves for different biasing voltages are presented in Fig.5.10, and the most important figures of merit are collect in Tab.5.4. Cells were always characterized without the application of a constant bias: measurements were performed immediately after (for example identified as "+3V" and "-3V" in Fig.5.10) or after 2 minutes (identified as "0V after -3V" and "0V after+3V").

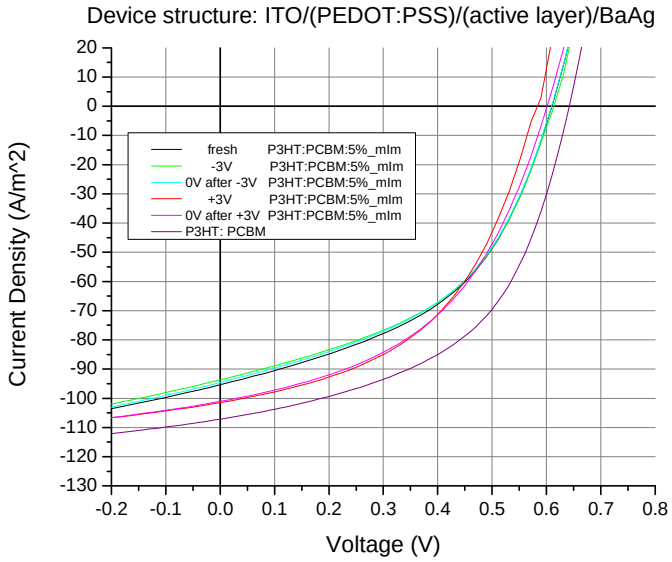

Fig.5.10 IV curve of fresh and biased P3HT:PCBM:5%mIm cell, firstly biased with -3V.

Tab.5.4 Parameters of fresh and biased P3HT:PCBM:5%mIm cell firstly biased with -3V.

P3HT:PCBM:5%mIm	V_{oc} [mV]	I_{sc} [A m^{-2}]	FF [%]	η
Fresh	610	-95	47	2.74
-3V	613	-93	48	2.71
0V after -3V	610	-95	47	2.71
+3V	584	-101	48	2.85
0V after +3V	601	-101	47	2.86

Thickness [nm]	T annealing [°C]	t annealing [min]
197	135	20

A 2 minute negative bias of the cell seems to have no significant effect on the performance parameters, which are only slightly decreased. On the other hand, the application of a positive bias leads to a small overall improvement of the power conversion efficiency. After a positive bias, V_{oc} is reduced by about 20 mV whereas the current

density is increased. A following measurement, 2 minutes after the bias application, shows that the improvement in I_{sc} is retained, accompanied by a partial re-establishing of the open circuit voltage (last enter of Tab.5.4). The influence of the sequence of bias applications was also investigated. Fig.5.11 shows the characteristics of a cell after the application of a reverse voltage sequence, that is, application of a positive bias first, followed by a negative one. The positive bias leads to the same performance increase as mentioned before. The negative voltage bias does not affect the cell behavior and it does not restore the performance of the fresh device.

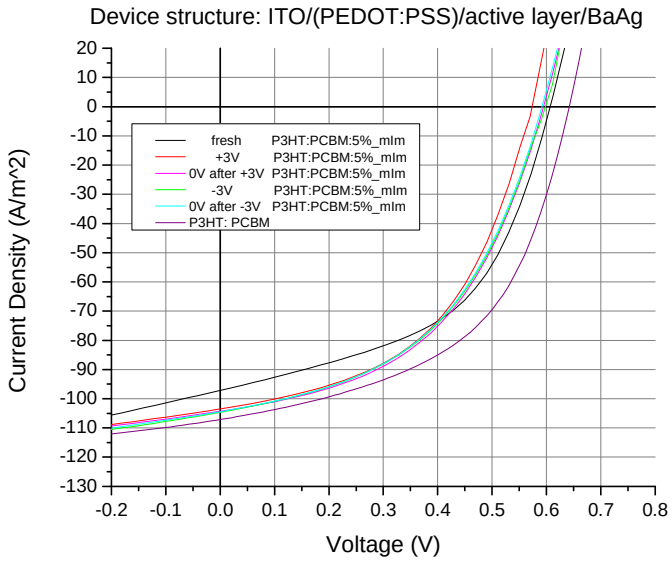

Fig.5.11 IV curve of fresh and biased P3HT:PCBM:5%mIm cell, firstly biased with +3V.

Another observed effect is the variation of the current density with the biasing time, depicted in Fig.5.12 and Fig.5.13. The current density is measured under light exposure during 2 minutes. The application of the bias produces an increase, or a decrease, on the current density for a positive, or for a negative bias, respectively. A steady state is reached after almost 60 seconds of biasing, hence the 2 minutes biasing used above appears to be sufficiently long. This type of behavior was already reported in LECs devices and also in bilayer planar heterojunction using ionic dyes by Lenes and Bolink (43). The value of the current density is obviously different, in line with the characteristics of the diode: a negative voltage is equivalent to a reverse bias of the diode and the conduction is very weak, while a positive bias induces a forward bias of the diode. The measure at 0 V shows no variation of the current, and this permits to excludes effect due to heating or others kinds of interactions.

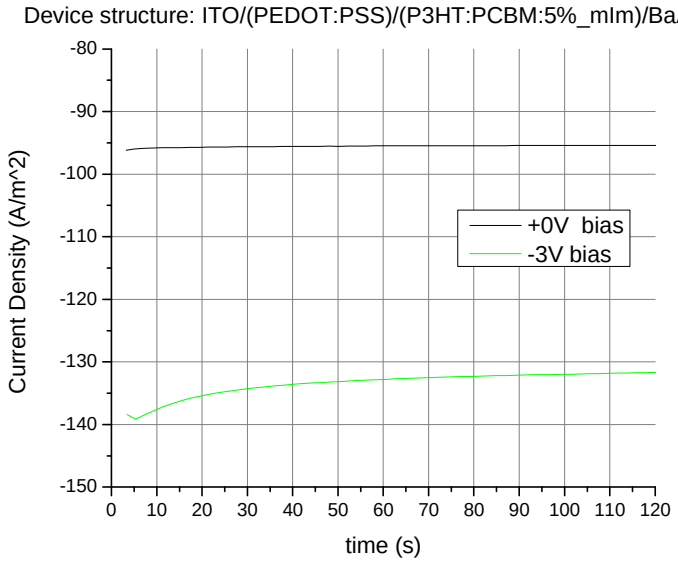

Fig.5.12 Current density dependence on the biasing time for a zero and a negative bias.

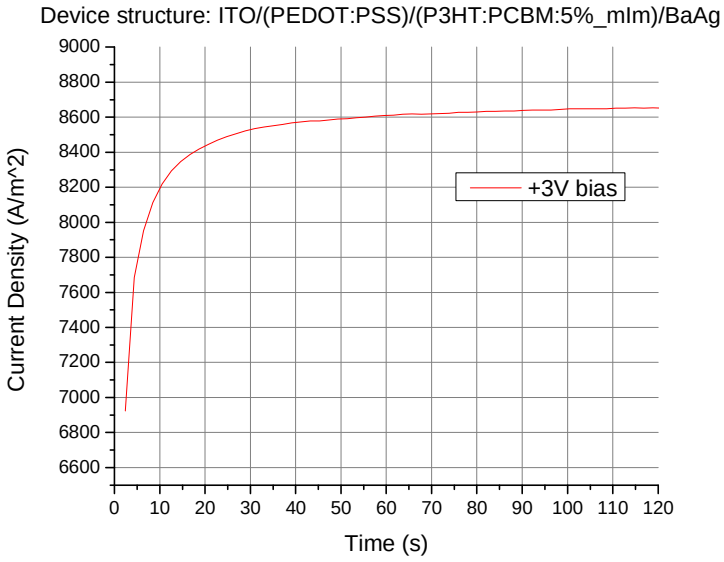

Fig.5.13 Current density dependence on the biasing time for a positive bias.

Some information can be drawn from the part of the IV curve of the cells in the negative voltage region (around short circuit condition). A zoom of this part of the IV curve of Fig.5.11 is shown in Fig.5.14. The addition of the ionic liquid to the blend gives rise to a cell with a different slope of the IV curve when compared with the P3HT:PCBM

reference device. For the device with the IL a higher slope is observed. It corresponds to a decrease of the shunt resistance which, as described in the previous section, is related with an increase of charge carrier recombination. Interestingly, after the application of the positive bias the slope of the curve decreases indicating that the recombination of charge carriers decreases. In organic semiconductors and excitonic devices complete charge carriers extraction occurs only at large negative voltages. As will be discussed below, the extraction is more efficient at lower light intensity conditions, where a complete extraction is possible and a flat line at I_{sc} is observed (see Fig.5.25). The application of a positive bias permits to improve the charge extraction and reduces the disadvantageous features of these cells.

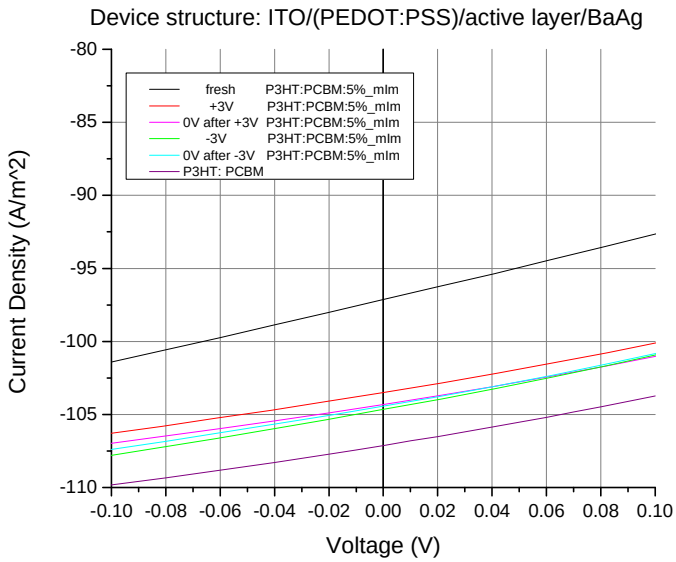

Fig.5.14 Zoom of IV curves of Fig.5.11 at I_{sc}.

Information about the mobility of charge carriers is obtained by looking at the positive voltage values, e.g. looking at the series resistor R_s (Fig.5.15). If compared with the P3HT:PCBM system, the addition of IL initially produces a decrease of the slope of the curve, which would indicate decrease in the charge carriers mobility. When a positive constant bias is applied, the cell shows a lower R_s, e.g. an increase charge carrier mobility, indicated by the increase of the slope of the IV curve at V_{oc}, even slightly better than the P3HT:PCBM reference. Such an increase in mobility would also be in agreement with the presence of doped regions, or a p-i-n junction. As mentioned before, mobility is also influenced by the morphology of the film: the size of the domain, the planarity and the order of the chains are only some characteristics that can be affected by the addition of an IL to the blend. Negative voltage biases do not give significant changes.

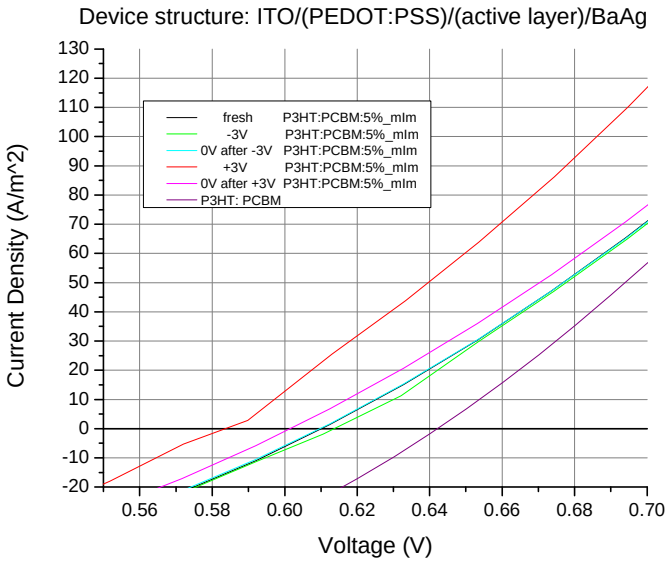

Fig.5.15 Zoom of IV curves shown in Fig.5.10 at V_{oc}.

Time is obviously an important variable in the movement of ions. As mentioned above, in the short bias tests, a period of 2 minutes was used. Ionic liquids are composed by ions with high molecular weight, and not by small size ions, such as metal ions. Thus, in addition to the results shown in Fig.5.12 and Fig.5.13, it is relevant to study the effect of longer biasing time. A +3V bias was applied for several hours, measuring the IV curve every 2h (Fig.5.16). The IV curve at 2 and 10 hours are not represented, because there was a crash of the software during the measurements. The initially fresh cell was not particularly good, but it is interesting to see the variation after the positive biasing. The application for a longer time gives the same kind of results described above for the short time, but the increase of the carriers mobilities and the reduction of carriers recombination are stronger. There is such an increase of the shunt resistance that it is possible to extract almost all the generated charges at I_{sc}, especially immediately after the biasing. The two effects combined give rise to an increase of FF, with a sharper curve, and thus a higher power conversion efficiency. In Tab.5.5 the characteristic values of the devices are listed. One can identify several interesting points:

- perfect overlapping of the curves after biasing, in the dark, for 4, 6, or 8 hours.
- Subsequent measurements of the cell, done after 5 minutes, give rise to higher performances in terms of both V_{oc} and I_{sc}. On the other hand, there is a systematic reduction in the FF
- A small increase of the performance after 24h from the last bias. Further measurements were not performed.

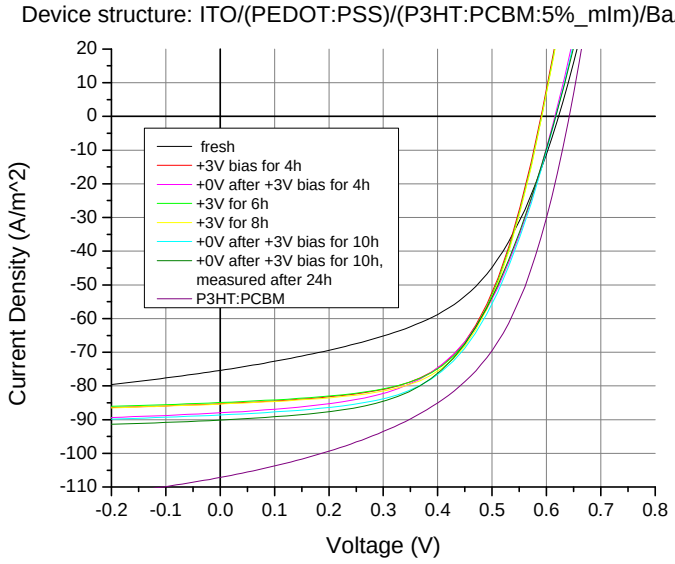

Fig.5.16 IV curve of fresh and +3V biased P3HT:PCBM:5%mIm cell, for different time.

Tab.5.5 Parameters of fresh and +3V biased P3HT:PCBM:5%mIm cell for different time.

P3HT:PCBM:5%mIm	V_{oc} [mV]	I_{sc} [A m^{-2}]	FF [%]	η	Thickness [nm]	T annealing [°C]	t annealing [min]
Fresh	623	-75	52	2.41	177	150	5
+3V for 4h	590	-85	61	3.04			
0V after +3V for 4h	616	-88	56	3.03			
+3V for 6h	591	-85	61	3.05			
+3Vfor 8h	592	-85	61	3.08			
0V after +3V for 10h	617	-89	57	3.11			
0V after +3V for 10h measured 24h later	617	-90	55	3.08			
P3HT:PCBM	642	-107	52	3.55	130	135	20

The application of a constant negative bias was performed too. After the application of a -3V for 2 hours, a decrease in the performance was observed, as depicted in Fig.5.17. This was expected, if an effective movement of ions is occurring. V_{oc} remains almost constant, whereas I_{sc} decreases, and thus the efficiency diminish. The curves obtained for longer negative bias, and even 5 minutes after the biasing, are perfectly overlapping the one obtained after 2 hours. These observations are opposite to those obtained for positive bias. In Tab.5.6, the values of the parameters of the curves are summarized.

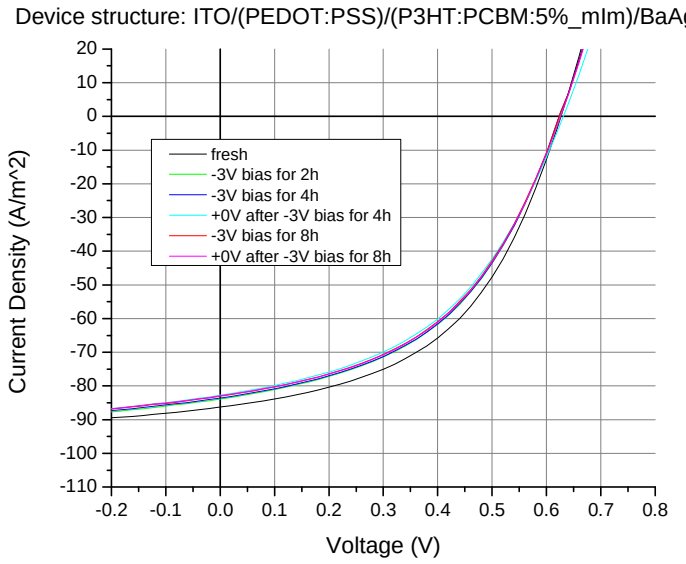

Fig.5.17 IV curve of fresh and -3V biased P3HT:PCBM:5%mIm cell, for different time.

Tab.5.6 Parameters of fresh and -3V biased P3HT:PCBM:5%mIm cell for different time.

P3HT:PCBM:5%mIm	V_{oc} [mV]	I_{sc} [A m^{-2}]	FF [%]	η
Fresh	627	-86	49	2.65
-3V for 2h	624	-84	47	2.48
-3V for 4h	624	-83	48	2.47
0V after 3V for 4h	631	-83	46	2.41
-3V for 8h	624	-83	47	2.44
0V after -3V for 4h	627	-83	47	2.45

Thickness [nm]	T annealing [°C]	t annealing [min]
177	150	5

Considering all the collected data, it is possible to develop a model able to describe the data obtained after biasing. The more interesting effects are:

- The application of a positive bias produces an increase in I_{sc} and in mobility of charge carriers, and a decrease in V_{oc} and non geminate recombination. At longer bias the effect is stronger than for short biasing.
- The application of a negative bias for a short time is not affecting the performance. At long biasing time, a reduction in I_{sc} is observed.
- The order of multiple biasing has influence on the cell performance, and there is no recovery in a short time.

In order to explain these effects, it is necessary to consider the energy levels of the components of the device before and after the connection of the electrodes, as depicted in Fig.5.18 and Fig.5.19 respectively. The contact between two different electrode materials produces an exchange of charge carriers which causes an alignment of the Fermi levels. The alignment of the Fermi levels of the metal electrodes produces the consequent tilting (also indicated as bending or shifting, according to the preferred interpretation of the phenomenon) of the semiconductors molecular orbitals levels. In an organic photovoltaic cell, after absorption of light, excitons generation and dissociation, the free charges are reaching the electrodes due to the built-in voltage, V_{bi}, which creates a potential drop across the cell. As described in the previous sections, electrons move through the PCBM molecules and holes are transported by the P3HT chains. Before entering the external circuit, charges have to cross the active layer/electrodes interfaces, which can be hindered by an energetic gap. (PEDOT:PSS)/P3HT HOMO and Ba/PCBM LUMO should create favorite contacts to holes and electrons extraction respectively. It should be mentioned that there are no method to measure the Fermi levels of organic semiconductors, thus it is assumed that there is vacuum level alignment.

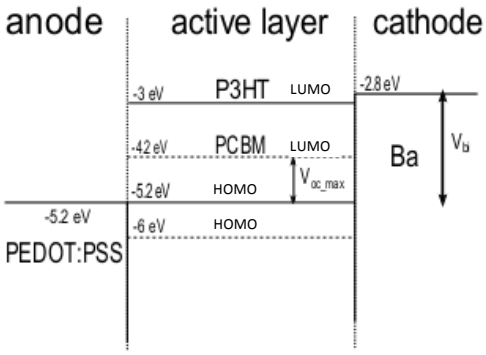

Fig.5.18 Energy levels, before contact of the electrodes, of the materials used in the fabricated device.

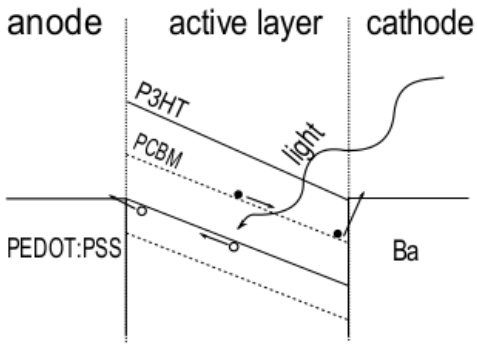

Fig.5.19 Energy levels, after contact of the electrodes (no bias applied), of the materials used in the fabricated device. Light absorption, exciton formation and separation, and collection of free charge carriers to electrodes are also depicted.

The application of a positive bias induces the movements of cations toward the cathode and anions to the anode. The accumulation of ions in the two zones gives rise to the electrochemical doping. The formation of the p- and n-regions which possess higher conductivity leads to a reduction of the intrinsic layer thickness. As a result the effective field is stronger over the intrinsic region, being the potential drop larger over the region with highest resistance, which leads to an increase in the charge mobility and a faster dissociation of the charge transfer states into free carriers, and consequently to a reduction of charges recombination.

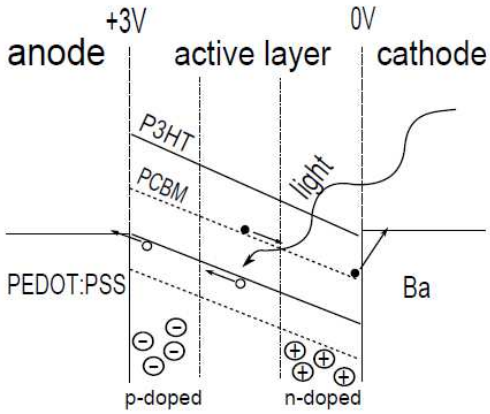

Fig.5.20 Formation of p-i-n structure after application of +3V bias. A p-doped region is created close to the anode, and a n-doped region close to cathode. Between the two, there is the intrinsic layer.

The overall effect is the generation of a higher current density, as experimentally observed. We do not have at present, an explanation for the decrease in V_{oc}. The movement of ions is dependent on the time of biasing, which is why the effect is larger after longer bias. Two hours of constant voltage biasing leads to a steady state condition, and no further effects that we could associate to ions movements are registered for longer biasing.

A negative bias produces a decrease of performance, only noticeable after long constant voltage application. Now, the accumulation of cations occurs at anode and the anions move to cathode. The built structure is not improving the charge carriers transportation to the correct electrode and, in principle, should produce more recombination.

The effects described above are related to the variations on the cell performance before and after the application of a constant bias to donor/acceptor/ionic liquid blends. The results obtained can be explained by the formation of doped zones, but perhaps other explanations may exists as well. However, the preparation of a P3HT:PCBM:1%bAm cell with an Al cathode after biasing at different voltage for 2 min sheds some light on the matter (Fig.5.21). An increase in cell PCE is observed after the application of a +3V, yet a strong decrease of PCE is registered after +5V constant voltage bias. At the +3V bias, the I_{sc} current is lower than in the fresh condition. This

may be related with the use of Al instead of Ba/Ag, as that leads to a lower build-in voltage of the cell. Yet the overall gain in power conversion efficiency is due to the increase in mobility by the formation of p- and n- regions, and the decrease of non geminate recombination.

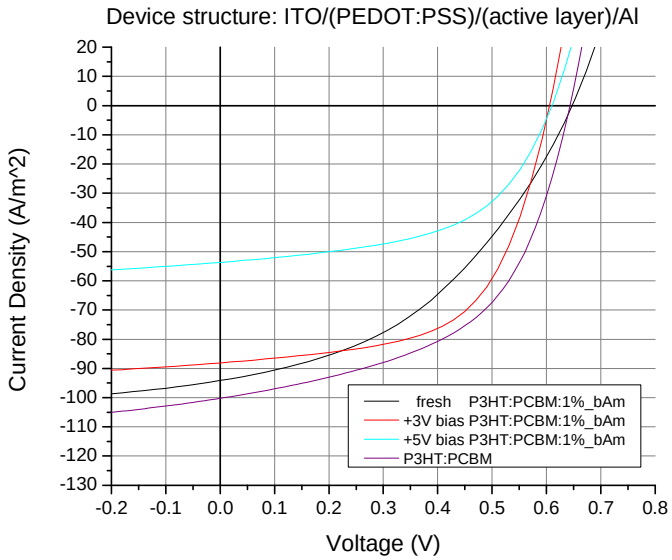

Fig.5.21 IV curve of fresh and biased P3HT:PCBM:1%bAm cell, at different bias voltages.

Tab.5.7 Parameters of fresh and biased cell, at different biases.

P3HT:PCBM:1%bAm	V_{oc} [mV]	I_{sc} [A m^{-2}]	FF [%]	η
Fresh	647	-94	42	2.58
+3V	606	-88	59	3.17
+5V	610	-53	54	1.76
P3HT:PCBM	643	-100	53	3.41

Thickness [nm]	T annealing [°C]	t annealing [min]
173	150	5
183	150	5

The apparently controversial effect of a positive bias can be explained considering the phenomena acting in the photocurrent generation and carriers extraction, and their different strength at different voltage values:

- Excitons are neutral species, bound electron and hole pairs, but, due to spatial distance between the two charges, an electric field is influencing their separation. The higher the external electric field the more probable will be the excitons dissociation
- The p- and n- regions, produced by the applied external electric field, present high conductivity of one kind of charge carrier but also present large quenching phenomenon. Quenching is stronger with increasing size of the p- and n- regions.

The behavior of the cell biased at +5V is completely different. If indeed doping occurs, it is possible that at 5 V the doped regions extend much further into the active layer. This would improve the possibility of exciton quenching, competing with the exciton dissociation process. It has been reported that doped layers are efficient exciton quenchers. Hence, with wide p- and n- regions exciton quenching would increase leading to a strong decrease of extractable current and thus of PCE. This experimental evidence is another hint of the formation of a p-i-n structure. Besides, a similar behavior was also reported using PPV and metal triflate salts, providing additional confirmation to our hypothesis (28).

In order to have a complete characterization of the device and to find additional evidence of the p-i-n formation by electrochemical doping, the characterization in the dark of P3HT:PCBM and P3HT:PCBM:5%mIm cells was performed. Constant voltages were applied for 2 minutes. In the P3HT:PCBM system, a progressive reduction of the threshold voltage of the diode with the increase of the positive applied bias is observed, as depicted in Fig.5.22.

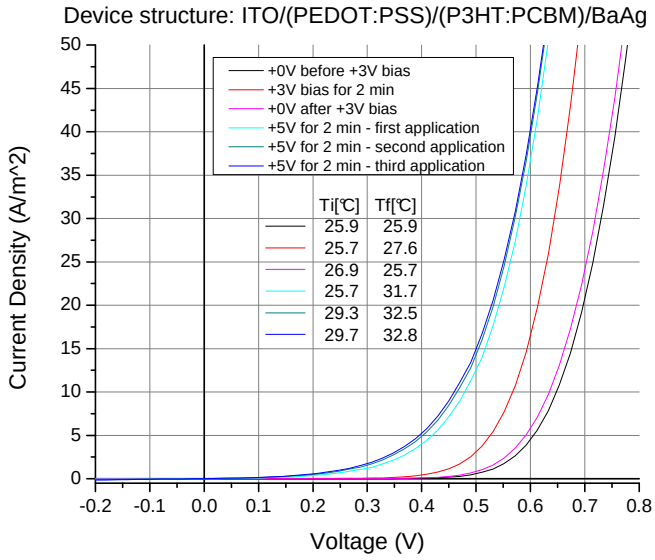

Fig.5.22 Biased IV curves of standard P3HT:PCBM cell in the dark at different bias voltages.

A different behavior was observed for a P3HT:PCBM:5%mIm, as shown in Fig.5.23. Here, an initial decrease of the threshold voltage is registered at +3V, while the subsequent application of a +5V bias produces a curve which lies between the fresh and the +3V IV curves.

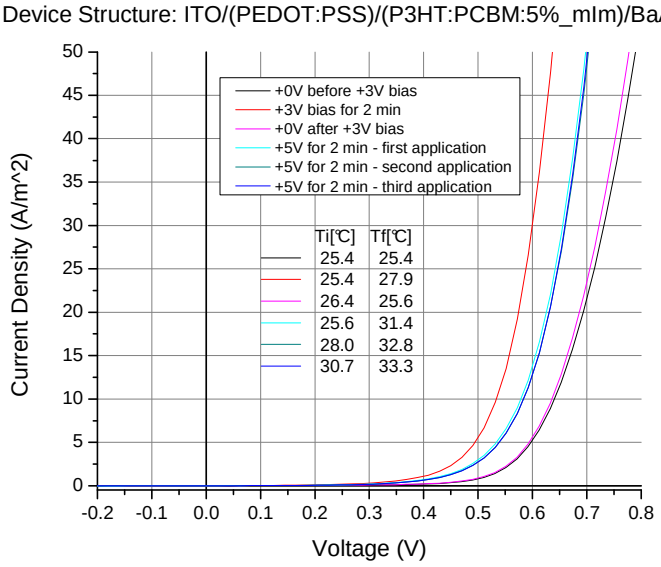

Fig.5.23 Biased IV curves of P3HT:PCBM:1%bAm cell in dark at different bias voltages.

The control of temperature variations before and after the application of each bias for both systems gave similar results. There was an increase of temperature of 7-8°C, with the maximum set around 33°C, in both cases. The increase of temperature could give rise to an increase in conduction, and thus explain the decrease of threshold voltage in P3HT:PCBM blend. The influence of temperature has to be present also in the cell with IL but, in this case, the p-i-n structure formation gives rise to different effects. In Fig.5.24 is possible to directly compare the curve at several voltage biases for the two systems. Considering that the fresh cells gave almost the same IV curves, it is possible to notice the larger displacement of the IV curve of the cell with IL in the blend after the application of the +3V. Besides, the IV curves after the application of +5V bias are shifted in opposite direction compared with the positions of the respective curves at +3V. The two experimental evidences may be related with the formation of the p-i-n structure, but further studies are required to understand the reasons for this different behavior.

Measurements of the two cells were performed at constant temperature, set at 25°C, in order to eliminate temperature influence. The application of a +3V bias produces a shift in P3HT:PCBM:5%mIm, as well as in P3HT:PCBM IV curves. Fig.5.25 shows the obtained results. In the latter, the displacement is much smaller than in P3HT:PCBM:5%mIm, and the formation of a p-i-n structure could explain this. Measures at +5V were not possible with this experimental apparatus. Further studies have to be performed in order to explain the unexpected shift of the IV curves observed in the P3HT:PCBM blend.

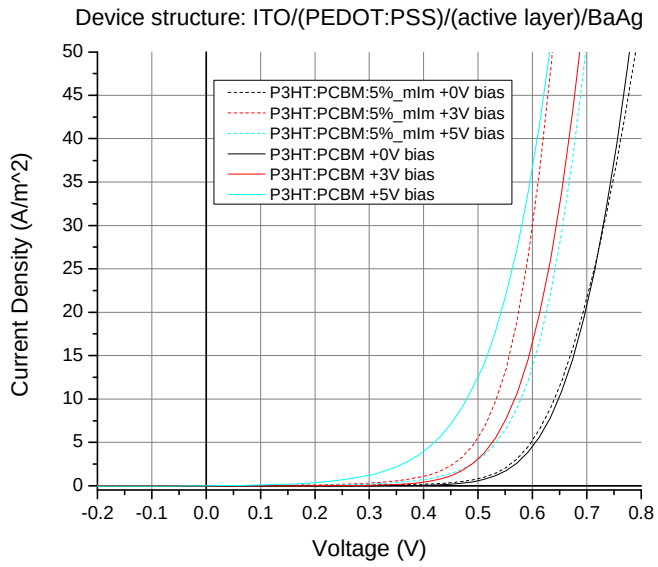

Fig.5.24 Comparison of biased IV curves of P3HT:PCBM and P3HT:PCBM:1%bAm cells in dark at different bias voltages.

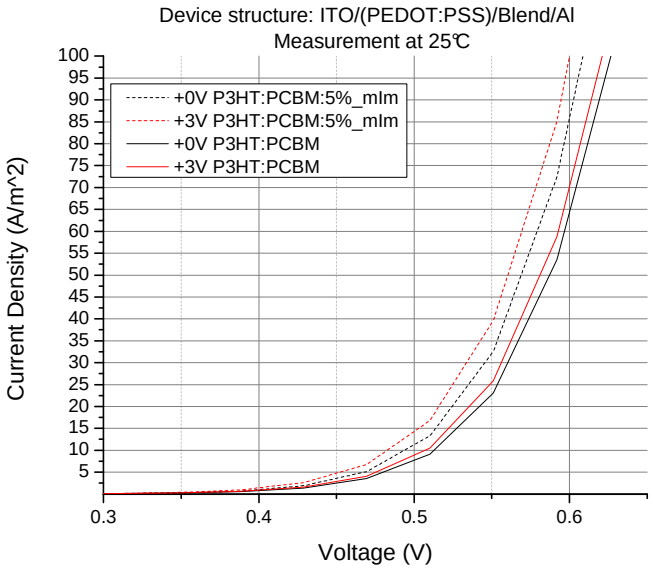

Fig.5.25 Comparison of IV curves of biased P3HT:PCBM and P3HT:PCBM:1%bAm cells in dark at different bias voltages at 25°C constant temperature.

Light intensity influence on cells performance

Interesting results were obtained from the comparison of I vs V curves of P3HT:PCBM and P3HT:PCBM:5%mIm cells under different light intensities. Optical filters were used to reduce the light intensity incident on the cells' surface. The cells prepared for this experiment showed lower values of V_{oc} and I_{sc}: the cell containing the IL had a higher short circuit current than the standard P3HT:PCBM. A possible reason for this anomalous behavior is a problem during cathode deposition, maybe due to some impurities or due to contamination of the glove box atmosphere (there was a problem related to the H_2O and O_2 levels in the glove box during the fabrication) which could have led to barium oxidation. A bad contact between active layer and cathode will be created and could explain the reduced V_{oc} and the odd current values. Anyway, considering that both devices were produced in the same process and both show the same kind of hitch, some information can be extracted.

As describe above, excitonic devices suffer from non geminate recombination and the complete charge carriers extraction is not happening at 0V, as it requires higher negative voltage values. Reducing the light intensity, the excitons generation is reduced and thus recombination phenomena are less probable: a flattening of the curve was already reported in literature (44), and our data for P3HT:PCBM, in Fig.5.26, are in agreement with that.

The cell with P3HT:PCBM:5%mIm shows higher recombination phenomena at AM 1.5 as already discuss above, and, surprisingly, important phenomena are present also at low light intensity. After an initial decrease of the recombination using a filter with 50% transmission, green dots line in Fig.5.26, the curves at lower transmission are parallel, and the slope around 0 V is constant. A possible explanation for the IL cell behavior is the action of the ionic liquid as recombination centers, e. g. traps, for charge carriers. Ions can improve recombination through a trap-assisted mechanism: traps create energy levels in the bandgap which can maintain a charge carrier for an extended time, rather than be extracted quickly, and make the recombination more probable. This may explain the initial decrease of recombination at 50% transmittance, happening when there is still abundance of charge carriers, and the further constant slope of the curves, which is determined by the ions concentration instead of the photogenerated charges. This should be particularly important for a bulk heterojunction, which is an architecture suffering from charge carriers extraction limitations.

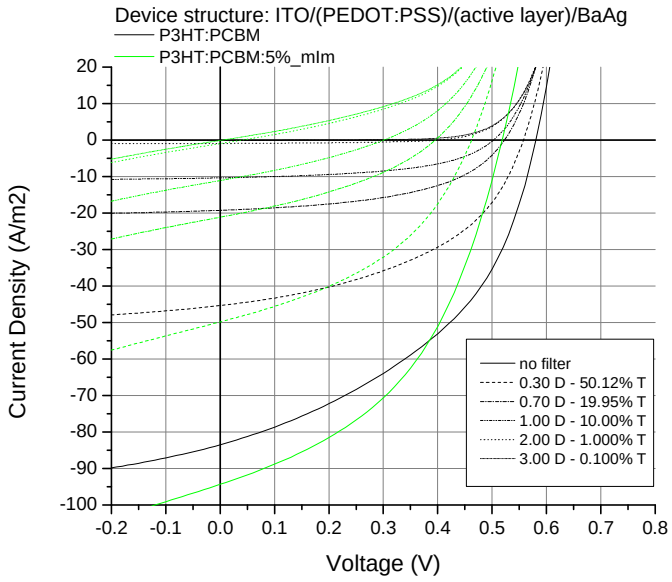

Fig.5.26 Comparison of IV curves of unbiased P3HT:PCBM and P3HT:PCBM:1%bAm cells at different light intensity.

Optimization

An attempt of cell optimization was done, trying to maximize cells performance. Several parameters affecting cell performance are analyzed: IL used, IL concentration and active layer thickness.

Fig.5.27 shows the influence of the IL concentration on cells performance. A clear worsening of cells behavior is registered with the increase of IL concentration in the blend. Tab.5.8 contains the parameters obtained from the IV curves.

Tab.5.8 Parameters of fresh P3HT:PCBM:mIm cells at different IL concentrations.

	V_{oc} [mV]	I_{sc} [A m^{-2}]	FF [%]	η
P3HT:PCBM:5%mIm	608	-93	52	2.91
P3HT:PCBM:10%mIm	606	-68	43	1.74
P3HT:PCBM:50%mIm	539	-37	25	0.51
P3HT:PCBM:100%mIm	439	-21	27	0.26

Thickness [nm]	T annealing [°C]	t annealing [min]
197	135	20
169	135	20
184	135	20
201	135	20

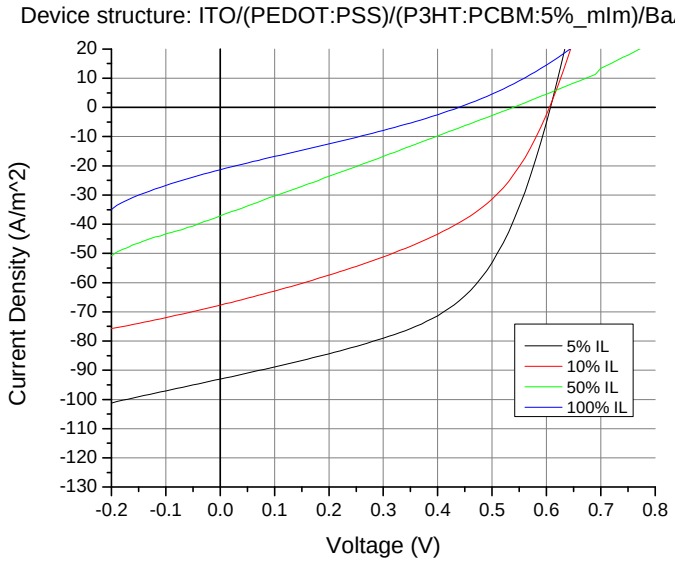

Fig.5.27 Comparison of IV curves of fresh P3HT:PCBM:mIm cells at different IL concentrations.

As mentioned above, an increase in the IL concentration means also a decrease in the P3HT and PCBM contents, and thus, a decrease in light absorption. Fig.5.28 shows the absorption spectrum of P3HT:PCBM:5%mIm and P3HT:PCBM:1%bAm cells with different active layer thickness. The absorbance of layers with higher IL concentration is lower when comparing films with the same thickness. This difference is more pronounced for the thicker layers studied.

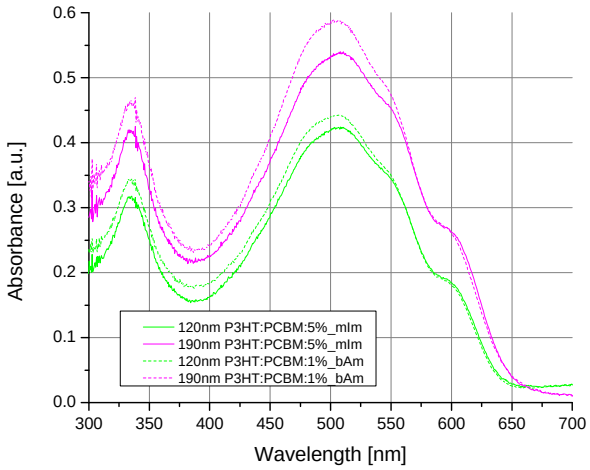

Fig.5.28 Absorption spectrum of P3HT:PCBM:5%mIm and P3HT:PCBM:1%bAm layers with different thickness.

The thickness of the active layer is an important factor affecting the power conversion efficiency of the cell, as described in the part regarding the physics of the device and the materials. In the fresh cell there are few factors related with the thickness of the cell that are affecting its performance. Basically, thickness influences the quantity of absorbed light and the path that free carriers must travel to reach the electrodes.

Fig.5.29 and Fig.5.30 represent the IV curves and the EQE of devices with 1% of tetra-n-butylammonium tetraphenylborate (bAm). Tab.5.9 contains the values of parameters obtained from those curves. This IL choice is motivated by the better and more reproducible results obtained. In fact, cells with 5% of 1-butyl-3-methylimidazolium hexafluorophosphate show a more complex behavior. S-shape IV curves were observed in some cases, and worst layer homogeneity was directly visible by the naked eye (especially in thicker layers). Fig.5.31 shows the different homogeneity of the layer in the two cases for 190 nm active layer devices. In order to have an ultimate comparison on samples surface homogeneity, tests with 1% of 1-butyl-3-methylimidazolium hexafluorophosphate should have been performed.

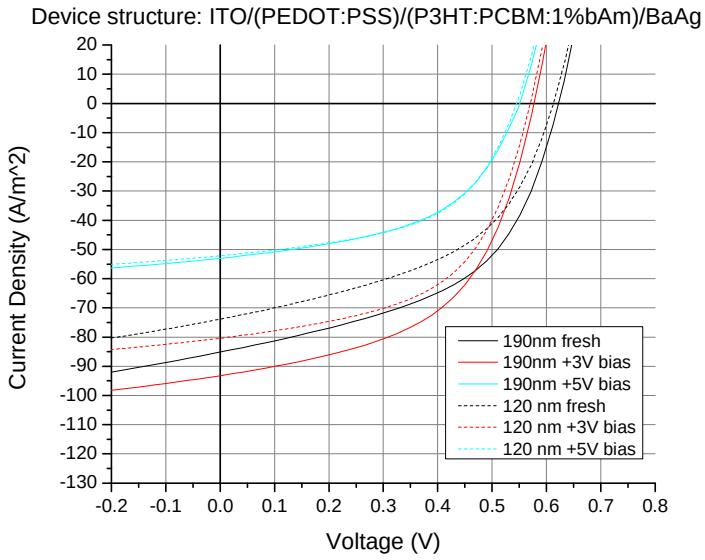

Fig.5.29 IV curve of fresh and biased P3HT:PCBM:1%bAm cells with different thickness at different bias voltages.

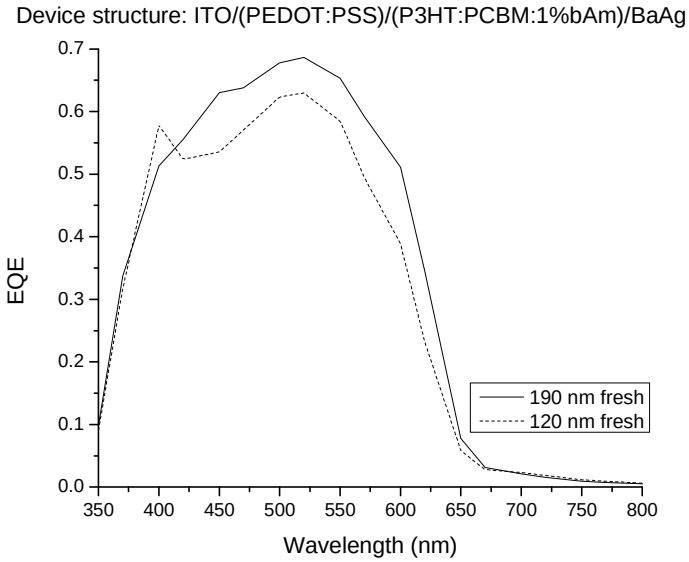

Fig.5.30 EQE curves of fresh P3HT:PCBM:1%bAm cells with different thickness.

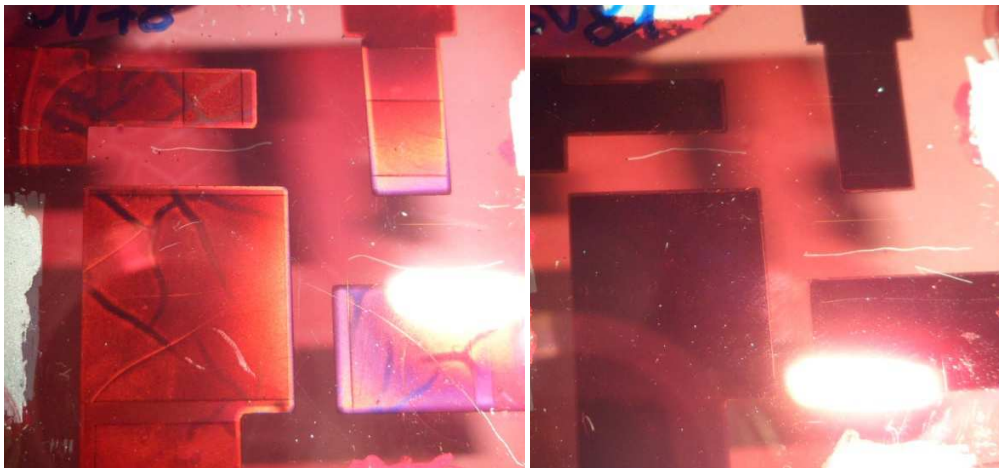

Fig.5.31 Homogeneity of 190nm active layers. On the left P3HT:PCBM:5%mIm, and on the right P3HT:PCBM:1%bAm.

Tab.5.9 Parameters of fresh and biased P3HT:PCBM:1%bAm cells with different thickness at different biases.

P3HT:PCBM:1%bAm	V_{oc} [mV]	I_{sc} [A m^{-2}]	FF [%]	η
120nm Fresh	613	-74	48	2.18
120nm +3V	570	-80	55	2.49
120nm +5V	545	-52	53	1.51
190nm Fresh	622	-85	51	2.69
190nm +3V	577	-93	53	2.85
190nmn +5V	550	-53	51	1.49

Thickness [nm]	T annealing [°C]	t annealing [min]
122	150	5
185		

Comparing the fresh cells, a higher PCE is obtained in the thicker cell. The higher current density is due to the larger absorption given by the presence of a higher amount of P3HT in the active layer. A look at the EQE plots, Fig.5.30, confirms the higher ability to convert photons in charge carriers for the thicker layer, even if 190 nm layer suffers larger recombination processes than the thin cell. After application of a +3 V bias, a slightly higher PCE is obtained for both thicknesses, remaining the thicker cell with higher efficiency. The thickness seems not to affect significantly the p-i-n structure formation, and the much higher PCE of the 190 nm active layer cells is mainly related to the higher performance of the fresh cell. At +5V, a decrease in performance is registered for both thicknesses, and the IV curves present an unexpected good, almost perfect, overlapping between them (in Fig.5.29). A further study on this could be very interesting. It seems evident that the cell with a thickness around 190 nm presents better behavior than the one of 120 nm. V_{oc} is, as expected, not affected by the thickness.

Concluding, Fig.5.33 shows the best result we obtained considering all the parameters discussed above. The cell is produced adding a 1% of tetra-n-butylammonium tetraphenylborate to a P3HT:PCBM blend and evaporating a BaAg cathode. The thickness is 190 nm, and a bias of +3V was applied for several hours. Measurements performed days after the bias application show the above mentioned improvement, and the cell seems to have a good stability from days up to weeks. In the end, it was possible to obtain a PCE of 3.64%, slightly better than the P3HT:PCBM used as reference. The improvement induced by the +3V bias is remarkable, with an increase in performance of almost 35% comparing with the fresh cell.

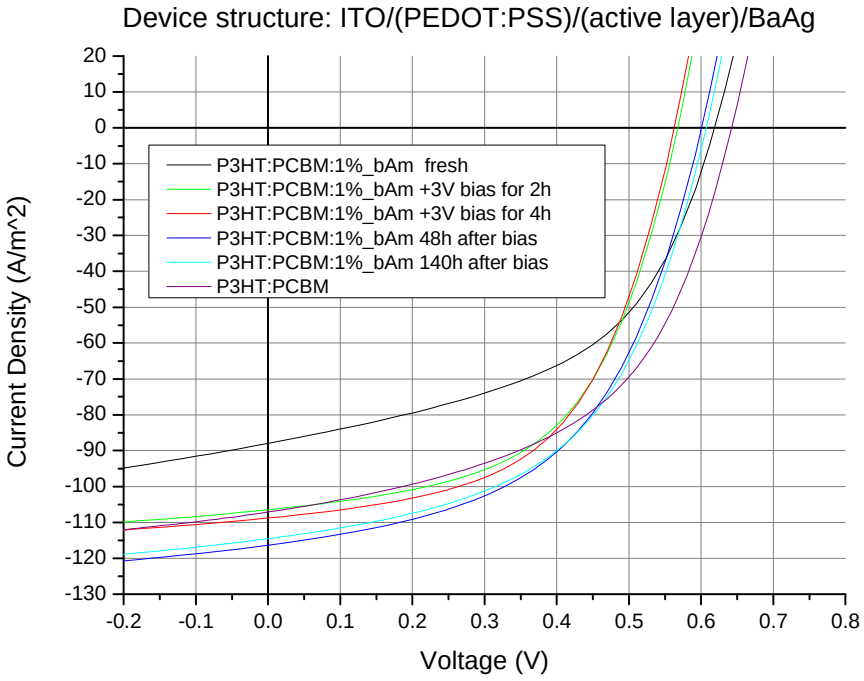

Fig.5.32 IV curves for fresh and biased different time in optimized device.

Tab.5.10 Parameters of fresh and biased cells for different time in a device with optimized structure.

P3HT:PCBM:1%bAm	V_{oc} [mV]	I_{sc} [A m^{-2}]	FF [%]	η	Thickness [nm]	T annealing [°C]	t annealing [min]
Fresh	619	-88	50	2.72	185	150	5
+3V for 2h	567	-106	55	3.31			
+3V for 4h	563	-109	55	3.36			
0V after +3V for 4h measured 48h later	600	-117	52	3.63			
0V after +3V for 4h measured 140h later	607	-115	52	3.64			
P3HT:PCBM	642	-107	52	3.55	130	135	20

Chapter 6 – Conclusions

Using two chemically compatible ionic liquids it was possible to prepare ion containing bulk-heterojunction solar cells based on a blend of P3HT and PCBM. The performance of the devices deteriorates with the addition of the ionic liquids, proportionally with the amount added. The reasons for this decrease were not yet determined but they are likely related with a reduction of the absorption, disruption of the crystalline packing of the P3HT and PCBM phases leading to increased recombination and reduced charge carrier mobilities. Yet, an increase in the solar cell performance was obtained after applying a positive bias. This increase intensified with prolonged biasing times. Negative biases did not lead to a significant change in the performance of the solar cells.

Direct evidence of the formation of a p-doped, intrinsic and an n-doped regions was not obtained. Yet several results can be explained in the framework of the p-i-n structure. The increase in current density and the improvement of the fill factor are some of them. Also the change in the slope of the curve close to V=0 and to the V_{oc} after positive bias indicate a reduction of the recombination and an increase in the charge carrier mobilities, which can be explained by the formation of highly conductive doped regions adjacent to the electrodes. Furthermore, when the applied bias is too high, no increase in current density and power conversion efficiency is obtained. This might mean that the doped regions have grown over too large distances causing a significant amount of excitons to be quenched prior to the formation of charge transfer states across the P3HT/PCBM interface.

Therefore, it appears possible that a p-i-n junction is formed in the ion containing P3HT:PCBM solar cells.

For the solar cell in which 1% of tetra-n-butylammonium tetraphenylborate was added the PCE obtained after positive biasing at 3 volts increased by 35% over the unbiased cell. More importantly, perhaps, is that the PCE obtained was higher than the ion-free P3HT:PCBM reference cell.

Chapter 7 -
Future developments

The work reported in this thesis is only a starting point for the study of the p-i-n formation in solar cells by electrochemical doping. All the addressed topics should be better explored, in order to obtain a better understanding of the physic of the devices. Many other aspects should be investigated, such as:

- Effort to reduce the initial performance decrease, in order to better exploit the increase of PCE after p-i-n formation. A deeper analysis on the optimization parameters (IL concentration, active layer thickness and IL used) is crucial.
- Further studies on current density dependence on biasing time, in order to understand ions migration and its effect along time.
- Study of the current density variations with light exposure time.
- Better understand of the relation between IL concentration with active layer absorbance and change in morphology. The distribution of the ions in the blend has also to be investigated.
- Study the changes in the morphology with the application of the bias.
- Replace PEDOT:PSS by MoO_3 as anode. PEDOT:PSS contains sodium ions which in principle could also migrate. Their movements complicate the study of the behavior of the cell, and it could alter its response.
- Use of low bandgap donor materials, such as poly[N-9'-heptadecanyl-2,7-carbazole-alt-5,5-(4',7'-di-2-thienyl-2',1',3'-benzothiadiazole)] (PCDTBT), and study the possibility to further improve the performance in donor/acceptor blends with high PCE.
- Study the influence of light intensity on the cell performances. In particular, cell characterization should be made after application of a bias.
- Possibility to apply a bias during the annealing treatment, in order to facilitate ions movements. Further knowledge of the relation between ions mobility and morphology of the layer is needed, considering that the annealing temperature affect both.

References

1. *Polymer-fullerene bulk heterojunction solar cells.* **C. Deibel, V. Dyakonov.** 2010, Report on Progress in Physics, Vol. 73.

2. **J. Poortmans, V. Arkhipov.** *Thin Film Solar Cells Fabrication, Characterization and Applications.* s.l. : Wiley, 2007.

3. *An "all-organic" battery: Single electron transfer in an electrochemical cell.* **E. M. Arnett, L.G. Whitesell Jr., J. P. Cheng, E. Marchot.** 13, Tetrahedron Letters, Vol. 29, pp. 1507-1508.

4. *Electroluminescence from polyvinylcarbazole films: 1. Carbazole cations.* **R.H.Partridge.** 6, 1983, Polymer, Vol. 24, pp. 733-738.

5. *Electroluminescence from polyvinylcarbazole films: 3. Electroluminescent devices.* **R.H.Partridge.** 6, 1983, Polymer, Vol. 24, pp. 748-754.

6. *Field-effect transistor with polythiophene thin film.* **H. Koezuka, A. Tsumura, T. Ando.** 1-3, 1987, Synthetic Metals, Vol. 18, pp. 699-704.

7. *Polymer Light-Emitting Electrochemical Cells.* **Q. Pei, G. Yu, C. Zhang, Y. Yang, A. J. Heeger.** 5227, 1995, Science, Vol. 269, pp. 1086-1088 .

8. *Organic photovoltaic films.* **J. Nelson.** 1, 2002, Current Opinion in Solid State and Materials Science, Vol. 6, pp. 87-95.

9. *Flexible organic P3HT:PCBM bulk-heterojunction modules with more than 1 year outdoor lifetime.* **J. A. Hauch, P. Schilinsky, S. A. Choulis, R. Childers, M. Biele, C. J. Brabec.** 7, 2008, Solar Energy Materials and Solar Cells, Vol. 92, pp. 727-731.

10. **Karl Leo.** Organic Semiconductor World. [Online] November 2011. http://www.orgworld.de/.

11. **M. Pope, C. E. Swenberg.** *Electronic processes in organic crystals and polymers.* s.l. : Oxford University Press, 1999.

12. *Molecular Understanding of Organic Solar Cells: The Challenges.* **J. Bredas, J. E. Norton, J. Cornil, V. Coropceanu.** 11, 2009, Accounts of Chemical Research, Vol. 42, pp. 1691-1699.

13. *Nanoscale Morphology of Conjugated Polymer/Fullerene-Based Bulk- Heterojunction Solar Cells.* **H. Hoppe, M. Niggemann, C. Winder, J. Kraut, R. Hiesgen, A. Hinsch, D. Meissner, N. S. Sariciftci.** 10, 2004, Advanced Functional Materials, Vol. 14, pp. 1005-1011.

14. *P3HT/PCBM bulk heterojunction solar cells: Relation between morphology and electro-optical characteristics.* **P. Vanlaekea, A. Swinnenb, I. Haeldermans, G. Vanhoyland, T. Aernouts, D. Cheyns, C. Deibel, J. D'Haen, P. Heremans, J. Poortmans, J.V. Manca.** 14, 2006, Solar Energy Materials and Solar Cells, Vol. 90, pp. 2150-2158.

15. *Influence of nanomorphology on the photovoltaic action of polymer–fullerene composites .* **D. Chirvase, J. Parisi, J. C. Hummelen, V. Dyakonov.** Nanotechnology, 9, Vol. 15, p. 1317.

16. *Role of the Charge Transfer State in Organic Donor–Acceptor Solar Cells.* **C. Deibel, T. Strobel , V. Dyakonov.** 2010, Advanced Materials, Vol. 22, pp. 4097-4011.

17. *Design Rules for Donors in Bulk-Heterojunction Solar Cells—Towards 10 % Energy-Conversion Efficiency.* **Markus C. Scharber, David Mühlbacher, Markus Koppe, Patrick Denk, Christoph Waldauf, Alan J. Heeger, and Christoph J. Brabec.** 2006, Advanced Materials, 18, pp. 789-794.

18. *Basic materials physics of transparent conducting oxides.* **P. P. Edwards, A. Porch, M. O. Jones, D. V. Morganb,R. M. Perks.** 2004, Dalton Transactions, Vol. 19, pp. 2995-3002.

19. *Universal energy-level alignment of molecules on metal oxides.* **M. T. Greiner, M. G. Helander,W. Tang, Z. Wang, J. Qiu, Z. Lu.** 2012, Nature materials, Vol. 11.

20. *Effect of LiF/metal electrodes on the performance of plastic solar cells.* **C. J. Brabec, S. E. Shaheen, C. Winder, N. S. Sariciftci, P. Denk.** 2002, Applied Physics Letters, 7, Vol. 80, p. 1288.

21. *Two-layer organic photovoltaic cell.* **C.W.Tang.** 1986, Applied Physics Letters, Vol. 48, p. 183.

22. *Efficient photodiodes from interpenetrating polymer networks.* **J. J. M. Halls, C. A. Walsh, N. C. Greenham, E. A. Marseglia, R. H. Friend, S. C. Moratti, A. B. Holmes.** 1995, Nature, Vol. 376, pp. 498-500.

23. *Charge separation and photovoltaic conversion in polymer composites with internal donor/acceptor heterojunctions.* **G. Yu, A. J. Heeger.** 1995, Journal of Applied Physics, Vol. 78, pp. 4510-4515.

24. **Klaus Petritsch.** Organic Solar Cell Architectures. July 2000.

25. *Organic p-i-n solar cells.* **B. Maennig, J. Drechsel, D. Gebeyehu, P. Simon, F. Kozlowski, A. Werner, F. Li, S. Grundmann, S. Sonntag, M. Koch, K. Leo, M. Pfeiffer, H. Hoppe, D. Meissner, N.S. Sariciftci, I. Riedel, V. Dyakonov, J. Parisi.** 2004, Applied Physics A, Vol. 79, pp. 1-14.

26. *High efficiency organic solar cells based on single or multiple PIN structures.* **J. Drechsel, B. Mannig, F. Kozlowski, D. Gebeyehu, A. Werner, M. Koch, K. Leo, M. Pfeiffer.** 2004, Thin Solid Films, Vols. 451-452, pp. 515-517.

27. *Polymer p-i-n Junction Photovoltaic Cells.* **J. Gao, G. Yu, A. J. Heeger.** 1998, Advanced Materials, 9, Vol. 10, pp. 692-695.

28. *In situ electrochemical doping enhances the efficiency of polymer photovoltaic devices.* **M. Su, H. Su, C. Kuo, Y. Zhoua, K. Wei.** 2011, Journal of Materials Chemistry, Vol. 21, pp. 6217-6224.

29. *Laminated fabrication of polymeric photovoltaic diodes.* **M. Granstrom, K. Petritsch, A. C. Arias, A. Lux, M. R.Andersson and R. H. Friend.** 1998, Nature, 395, pp. 257-260.

30. **Halls, J. J. M.** Photoconductive properties of conjugated polymers. Cambridge : s.n., 1997. PhD thesis.

31. *Current-Voltage Characteristics of Bulk Heterojunction Organic Solar Cells: Connection Between Light and Dark Curves.* **P.P. Boix, A. Guerrero, L. F. Marchesi, G.Garcia-Belmonte,J. Bisquert.** 2011, Advanced Energy Materials, Vol. 20, pp. 1-6.

32. *Ex-ante environmental and economic evaluation of polymer photovoltaics.* **A. L. Roes, E. A. Alsema, K. Blok, M. K. Patel.** 2009 : s.n., Progress in Photovoltaics, Vol. 17, pp. 372-393.

33. *Polymer solar cells.* **G. Li, R. Zhu, Y. Yang.** 2012, Nature photonics, Vol. 6.

34. *A strong regioregularity effect in self-organizing conjugated polymer films and high-efficiency polythiophene:fullerene solar cell.* **Y. Kim, S. Cook, S. M. Tulandhar, S. A. Choulis, J. Nelson, J. R. Durrant, D. D. Bradley, M. Giles, I. McCulloch, C. Ha, M. Ree.** 2006, Nature Materials, Vol. 5, pp. 197-203.

35. *Charge Transport and Photocurrent Generation in Poly(3-hexylthiophene):Methanofullerene Bulk-Heterojunction Solar Cells.* **V. D. Mihailetchi, H. Xie, B. De Boer, L. J. A. Koster, P. W. M. Blom.** 2006, Advanced Functionals Materials, Vol. 16, pp. 699-708.

36. *Investigation of annealing effects and film thickness dependence of polymer solar cells based on poly(3-hexylthiophene).* **G. Li, V. Shrotriya, Y. Yao, Y. Yang.** 2005, Journal of Applied Physics, Vol. 98.

37. *Effects of Postproduction Treatment on Plastic Soalr Cells.* **F. Padinger, R. S. Rittberger, N. S. Sariciftci.** 2003, Advanced Functional Materials, Vol. 13, pp. 1-4.

38. *Influence of the Blend Concentration of P3HT: PCBM in the Performances of BHJ Solar Cells.* **O. Ourida, B. M. Said.** 2011, Science Academy Transactions on Renewable Energy Systems Engineering and Technology, Vol. 1, pp. 90-92.

39. *Effect of Trace Solvent on the Morphology of P3HT:PCBM Bulk Heterojunction Solar Cells.* **L. Chang, H. W. A. Lademann, J. Bonekamp, K. Meerholz, A. J. Moulé.** 2011, Advanced Functional Materials, Vol. 21, pp. 17779-1787.

40. **J. S. Wilkes, M. J. Zaworotko.** 1992, Chemical Communications, pp. 965-967.

41. *Ionic Liquid Doped Polymer Light-Emitting Electrochemical cells.* **C. Yang, Q. Sun, J. Qiao, Y. Li.** 2003, The Journal of Physical Chemistry B, Vol. 107, pp. 12981-12988.

42. *WSXM: A software for scanning probe microscopy and a tool for nanotechnology.* **I. Horcas, R. Fernández, J. M. Gómez-Rodríguez, J. Colchero, J. Gómez-Herrero, A. M. Baro.** 2007, Review of Scientific Instruments, Vol. 78, pp. 013705-1 - 013705-5.

43. *Ionic Space-Charge Effects in Solid State Organic Photovoltaics.* **M. Lenes, H. J. Bolink.** 2010, Applied Materials and Interfaces, 10, Vol. 2, pp. 3664-3668.

44. *Low Light Performance of Mono-Crystalline Silicon Solar Cells.* **G. Bunea, K. Wilson, Y. Meydbray, M. Campbell, D. D. Ceuster.** 2006, Photovoltaic Energy Conversion, Conference Record of the 2006 IEEE 4th World Conference, pp. 2312-2314.